

**NUMERICAL DETERMINATION OF
PERMEABILITY AND INTERFACIAL
CONVECTIVE HEAT TRANSFER COEFFICIENT
FOR NON-ISOTROPIC AND PERIODIC DUAL
SCALE POROUS MEDIUM**

**A Thesis Submitted to
the Graduate School of Engineering and Science of
İzmir Institute of Technology
in Partial Fulfillment of the Requirements for the Degree of**

MASTER OF SCIENCE

in Mechanical Engineering

**by
Safa SABET**

**June 2015
İZMİR**

We approve the thesis of **Safa SABET**

Examining Committee Members:

Assist. Prof. Dr. Murat BARIŐIK

Supervisor, Department of Mechanical Engineering, İzmir Institute of Technology

Prof. Dr. Moghtada MOBEDI

Faculty of Engineering, Shizuoka University

Assist. Prof. Dr. Ünver ÖZKOL

Department of Mechanical Engineering, İzmir Institute of Technology

Assist. Prof. Dr. Erdal ÇETKİN

Department of Mechanical Engineering, İzmir Institute of Technology

Prof. Dr. Aytunç EREK

Department of Mechanical Engineering, Dokuz Eylül University

25 June 2015

Assist. Prof. Dr. Murat BARIŐIK

Supervisor, Department of Mechanical Engineering, İzmir Institute of Technology

Prof. Dr. Moghtada MOBEDI

Co-Supervisor, Faculty of Engineering, Shizuoka University

Prof. Dr. Metin TANOĐLU

Head of the Department of Mechanical Engineering

Prof. Dr. Bilge KARAÇALI

Dean of the Graduate School of Engineering and Sciences

ACKNOWLEDGMENTS

I would never have been able to finish my dissertation without the guidance of my committee members, help from friends, and support from my family.

I would like to express my deepest gratitude to my supervisor Prof. Dr. Moghtada Mobedi for his excellent guidance, caring, patience and immense knowledge. His guidance helped me in all the time of research and writing of this thesis. I would like to thank my advisor Assist. Prof. Dr. Murat Barışık for providing me the opportunity to complete my Master of Science thesis at İzmir Institute of Technology. I especially want to thank him, whose support and guidance made my thesis work possible.

In particular, I would like to thank my dear friends Seda Ulusoy, Hasan Çelik and Türküler Özgümüş for their helps and supports. Also I would like to thank the members of room 142, Heat and Mass Transfer Lab. for their friendships.

Last but not the least, I take this opportunity to express the profound gratitude from my deep heart to my father Sadegh and my two valuable and unique sisters Parisa and Parinaz for their love, generous care and continuous support. They were always supporting and encouraging me with their best wishes. My sincere thanks also goes to my brother in law Hamidreza for his never ending support and motivation.

ABSTRACT

NUMERICAL DETERMINATION OF PERMEABILITY AND INTERFACIAL CONVECTIVE HEAT TRANSFER COEFFICIENT FOR NON-ISOTROPIC AND PERIODIC DUAL SCALE POROUS MEDIUM

In this study, the fluid flow and heat transfer in a periodic, non-isotropic dual scale porous media consisting of permeable square rods in inline arrangement is analyzed to determine permeability and interfacial convective heat transfer coefficient, numerically. A periodical representative elementary volume (REV) with the dimensions of $H \times H$ is chosen as the computational domain. The flow in the REV is assumed fully developed and periodical. The permeable square particles are placed with in-line arrangement. There are two symmetrical intraparticle pores considered here which are in longitudinal flow direction. The continuity, Navier-Stokes and energy equations are solved to obtain the velocity, pressure and temperature distributions in the unit structures of the dual scale porous media. The obtained fields are upscaled by using volume average method to obtain the intrinsic inter and intraparticle permeabilities, bulk permeability tensor, interfacial convective heat transfer coefficients and the corresponding Nusselt numbers of the dual scale porous media for different values of inter and intraparticle porosities. The study is performed for interparticle porosities between 0.4 and 0.75 and for intraparticle porosities range of 0.2 to 0.8. A correlation based on Kozeny-Carman theory in terms of interparticle and intraparticle porosities and permeabilities is proposed to determine the bulk permeability tensor of the dual scale porous media. The intraparticle porosity value increase the flow rate passes through the porous media and the particle becomes more permeable. However; for high interparticle porosity values, the intraparticle porosity does not have importance effect on bulk permeability. Additionally, the results predicts that the interfacial convective heat transfer coefficient increases with increase of Reynolds number and the ratio of intra to interparticle porosity, while the increase rate shows variation with the porosity ratio and Reynolds number values.

Keywords and Phrases: Dual scale porous media, Numerical simulation, Permeability, Interfacial convective heat transfer coefficient, porosity, Kozeny-Carman Equation

ÖZET

GEÇİRGENLİK VE ARAYÜZEY ISI TAŞINIM KATSAYISININ İZOTROPİK OLMAYAN, PERİYODİK VE ÇİFTE SEVİYE GÖZENEKLİ YAPI İÇİN SAYISAL OLARAK BELİRLENMESİ

Bu çalışmada, çizgi düzleminde geçirgen kare çubuklardan oluşan periyodik ve izotropik olmayan çifte seviye gözenekli ortamda akışkan akışı ve ısı transferi analizi yapılmıştır. Geçirgenlik ve arayüzey taşınım ısı transfer katsayısı sayısal olarak belirlenmiştir. Bir periyodik öz temsili hacim (ÖTH) $H \times H$ boyutlarında hesaplama alanı olarak seçilmiştir. ÖTH'deki akış tam gelişmiş ve periyodik varsayılmıştır. Geçirgen kare parçacıklar çizgi düzleminde yerleştirilmiştir. Uzunlamasına ve akış yönünde düşünülen iki simetrik parçacık içi gözenekler vardır. Süreklilik, Navier-Stokes ve enerji denklemleri çifte seviye gözenekli yapıda hız, basınç ve sıcaklık dağılımlarını elde etmek için çözülmüştür. Elde edilen sonuçlar parçacık içi ve arası geçirgenliği, toplu geçirgenlik tensörü, arayüzey taşınım ısı transferi katsayılarına karşılık gelen Nusselt sayılarını elde etmek için farklı parçacık içi ve arası gözeneklilik değerleri için hacimsel ortalama yöntemi kullanılarak elde edilmiştir. Çalışma, 0.4 ve 0.75 arasında parçacık içi gözeneklilik ve 0.2 ile 0.8 aralığındaki parçacık arası gözeneklilik için gerçekleştirilmiştir. Parçacık içi ve arası gözeneklilik ve geçirgenliği açısından Kozeny-Carman teorisine dayalı bir ilişki, çifte seviye gözenekli ortamın toplu geçirgenliği tensörünü belirlemek için önerilmiştir. Parçacık içi gözeneklilik değerinin yükselmesi, akışkanın debisini arttırmakla birlikte gözenekli yapının daha geçirgen olmasını sağlamaktadır. Bununla birlikte; yüksek parçacık arası gözeneklilik değerleri için, parçacık içi gözenekliliğin toplu geçirgenliğe önemli etkisi olmadığı gözlemlenmiştir. Ayrıca, elde edilen sonuçlara göre arayüzey ısı taşınım katsayısı, Reynold sayısının artması ve parçacık içi ve arası gözeneklilik oranı ile artar, artış oranı ise gözeneklilik oranı ve Reynold sayısı değerleri ile değişimini göstermektedir.

Anahtar Kelimeler ve Deyimler: Çift seviye gözenekli yapı, Sayısal simülasyon, geçirgenlik, Arayüzey ısı taşınım katsayısı, Gözeneklilik, Kozeny-Carman denklemi

TABLE OF CONTENTS

LIST OF FIGURES	ix
LIST OF TABLES	xi
LIST OF SYMBOLS	xii
CHAPTER 1. INTRODUCTION	1
1.1. Dual Scale Porous Medium	2
1.2. The Aim of Study	3
1.3. Literature Review	4
1.3.1. Literature Review on Permeability for Dual Scale Porous Media ..	5
1.3.2. Literature Review on Kozeny Constant	11
1.3.3. Literature Review on Interfacial Convective Heat Transfer Coefficient	13
1.4. The Outline of Thesis	18
CHAPTER 2. FUNDAMENTALS OF MACROSCOPIC HEAT AND FLUID FLOW ANALYSIS IN POROUS MEDIA	19
2.1. Microscopic and Macroscopic Views of Porous Media	19
2.2. Microscopic Fluid Flow and Energy Equations	21
2.3. Volume Averaging Method	23
2.4. Darcy and Forchheimer Motion Equations	24
2.5. General Forms of Macroscopic Motion Equations	27
2.6. Macroscopic Energy Equations	30

CHAPTER 3. CONSIDERED DOMAIN, GOVERNING EQUATIONS AND BOUNDARY CONDITIONS.....	34
3.1. Considered Domain	34
3.2. Governing Equations and Boundary Conditions for Determination of Permeability	36
3.2.1. Determination of Intrinsic Intraparticle Permeability	37
3.2.2. Determination of Intrinsic Interparticle Permeability	38
3.2.3. Determination of Bulk Permeability	39
3.3. Governing Equations and Boundary Conditions for Determination of Interfacial Convective Heat Transfer Coefficient	41
 CHAPTER 4. SOLUTION TECHNIQUE AND COMPUTATIONAL DETAILS.....	 43
4.1. Numerical Procedure	43
4.1.1. Iterative Procedure for Obtaining Periodical Fluid Flow Boundaries	43
4.1.2. Iterative Procedure for Obtaining Periodical Thermal Boundaries for Determination of Interfacial Convective Heat Transfer Coefficient.....	44
4.2. Computational Details	46
4.3. Grid Independency Tests	46
 CHAPTER 5. RESULTS AND DISCUSSION.....	 48
5.1. Validation of Results	48
5.2. Results for Permeability and Kozeny Constant.....	50
5.2.1. Permeability in x Direction	50
5.2.2. Permeability in y Direction	55
5.3. Suggested Correlations	58
5.4. Results for Interfacial Convective Heat Transfer Coefficient	61

5.4.1. Effects of Intraparticle Porosity on the Interfacial Nusselt Number	62
CHAPTER 6. CONCLUSION	69
REFERENCES	71

LIST OF FIGURES

<u>Figure</u>	<u>Page</u>
Figure 1.1. Schematic view of dual scale porous media.....	3
Figure 2.1. Schematic views of porous media	20
Figure 2.2. Macroscopic and microscopic flows through a porous channel.....	21
Figure 2.3. Microscopic control volume in a porous structure	23
Figure 2.4. Flow through a bundle of capillary tubes	25
Figure 3.1. The studied dual scale porous medium	34
Figure 3.2. Computational domains.....	35
Figure 3.3. REV with different intraparticle size.....	36
Figure 4.1. The change of velocity profile to obtain fully developed condition	44
Figure 4.2. The change of temperature profile to obtain thermally fully developed condition	45
Figure 4.3. The change of dimensionless permeability with grid number for two dual scale porous media; $\varepsilon_f = 0.75$, $\varepsilon_p = 0.2$ and $\varepsilon_f = 0.4$, $\varepsilon_p = 0.8$	47
Figure 5.1. Comparison of dimensionless permeability obtained in this study with the results reported in literature	48
Figure 5.2. Comparison of the obtained results for the change of interfacial Nusselt number with the results of the reported studies	49
Figure 5.3. Change of permeability with Reynolds number for two dual scale porous media; $\varepsilon_f = 0.75$, $\varepsilon_p = 0.2$ and $\varepsilon_f = 0.4$, $\varepsilon_p = 0.8$	50
Figure 5.4. The streamlines and pressure contours for flow in x direction in dual scale porous media with $\varepsilon_f = 0.75$	51
Figure 5.5. The streamlines and pressure contours for flow in x direction in dual scale porous media with $\varepsilon_f = 0.4$	52
Figure 5.6. The change of intrinsic interparticle, intraparticle and bulk permeabilities with intraparticle porosity	54
Figure 5.7. Change of $K_{b,xx} / K_{f,xx}$ with intraparticle porosity for different values of interparticle porosity	54
Figure 5.8. The change of $K_{b,xx} / D^2$ with $\varepsilon_f^3 / (1 - \varepsilon_f)^2$	55

Figure 5.9. The streamlines and pressure contours for flow in y direction in dual scale porous media with $\varepsilon_f = 0.75$	56
Figure 5.10. The streamlines and pressure contours for flow in y direction in dual scale porous media with $\varepsilon_f = 0.4$	57
Figure 5.11. The change of $K_{b,yy} / D^2$ with $\varepsilon_f^3 / (1 - \varepsilon_f)^2$	58
Figure 5.12. The comparison of suggested correlation in longitudinal direction with the obtained numerical permeability values	60
Figure 5.13. The comparison of the suggested equation for permeability in transverse direction with obtained numerical results.....	61
Figure 5.14. The streamlines and temperature contours for $\varepsilon_f = 0.75$	63
Figure 5.15. The streamlines and temperature contours for $\varepsilon_f = 0.4$	64
Figure 5.16. The variation of real Nu with ε_p for $\varepsilon_f = 0.75$ and different Re values.....	65
Figure 5.17. The variation of real Nu with ε_p for $\varepsilon_f = 0.6$ and different Re values	66
Figure 5.18. The variation of real Nu with ε_p for $\varepsilon_f = 0.4$ and different Re values	66
Figure 5.19. The ratio of modified Nusselt number* to Nu number of mono scale porosity porous of media with a) $\varepsilon_f = 0.75$, b) $\varepsilon_f = 0.6$, c) $\varepsilon_f = 0.4$	68

LIST OF TABLES

<u>Table</u>	<u>Page</u>
Table 1.1. The performed studies and suggested relations for determination of permeability in a dual scale porous media.....	9
Table 1.2. Theoretical studies on the determination of Kozeny constant.....	12
Table 1.3. Theoretical studies on the determination of interfacial convective heat transfer coefficient	16
Table 5.1. Empirical coefficients for determination of Kozeny constant ($0.4 < \varepsilon_f < 0.75$ and $0.2 < \varepsilon_p < 0.8$)	59

LIST OF SYMBOLS

C	Forchheimer coefficient	
d	Height of intraparticle pore	m
D	Size of square particle	m
h	Convective heat transfer coefficient	W/m ² K
H	REV dimension	m
k	Thermal conductivity	W/mK
K	Permeability	m ²
L	Characteristic length	m
\dot{m}	Mass flow rate	m/s
Nu	Nusselt number	
p	Pressure	Pa
Pe	Peclet number	
Pr	Prandtl number	
q''	Heat flux	W/m ²
Re	Reynolds number	
T	Temperature	°C
u	Velocity in x direction	m/s
\vec{u}	Velocity vector	m/s
u_D	Darcian velocity	m/s
v	Velocity in y-direction	m/s
V	Volume	m ³

Greek Letters

ε	Porosity	
θ	Dimensionless temperature	
κ	Kozeny constant	
μ	Dynamic viscosity	Ns/m ²
ν	Kinematic viscosity	m ² /s
ρ	Density	kg/m ³
ϕ	Any parameter	

Subscripts

b	Bulk
f	Fluid
ref	Reference
s	Solid
sf	Interfacial
w	Wall
p	Particle
xx	Longitudinal
yy	Transverse

CHAPTER 1

INTRODUCTION

A porous medium is a composite medium consists of solid and voids. The voids can be interconnected (open cell) or disconnected (closed cell). The fluid flow and heat transfer in porous media are significantly considered recently because of their wide applications in both nature and industrial area. The application of transport properties in porous media has encountered in many branches of engineering. Food and crop drying processes, chemical reactors, filters, membranes, gas separator adsorbent beds, nuclear reactors, and heat exchangers can be given as industrial examples in which transport in porous media shows up as fundamental point. In the nature, the flowing of water or petroleum through rocks and soil, air flowing in lung, blood flow in liver, biological tissues and veins or even flow of air in forests can be exhibited as cases for transport in porous media.

In an open cell porous medium, fluid flows through the pores (or voids) between the particles. The behavior of the flow through the pores is complex and the flow is three dimensional. Consequently, pore level determinations of the velocity and the temperature fields are troublesome. Therefore, to analyze heat and fluid flow in porous media some approaches are obliged to overcome the difficulties. One of the most common methods is the macroscopic approach which is a simple and practical method for determination of velocity and pressure fields in a porous medium. However, this method requires the macroscopic transport properties of the porous medium such as permeability (and Forchheimer coefficient for flows with high inertia effect). The permeability is a tensor quantity and it depends on the geometrical parameters of the porous media. It can be obtained numerically and/or experimentally. Recently, improvements in computer and software technologies facilitate the prediction of permeability of a porous medium by using pore scale computational approach. Porous media with simple geometrical parameters can be easily modelled in a computer while methods such as tomography techniques can be employed to obtain digital representation of a heterogeneous porous medium with complex pore shapes. The study of Nakayama et al. (Nakayama et al., 2002) who obtained the permeability for a two dimensional periodic isotropic porous media

consisting of square rods, Ozgumus et al. (Ozgumus et al., 2014) who studied the effect of pore to throat size ratio on permeability and Kozeny constant, are two samples for determination of permeability by using pore level computational approach.

1.1. Dual Scale Porous Medium

A dual scale porous medium is a porous structure in which the solid region is also permeable since it involves pores in which fluid can flow. A schematic view of a dual scale porous media is shown in Figure 1.1. As can be seen, there are two kinds of pores in a dual scale porous medium. The first type of pores which can be called as interparticle pores is the main pores of the porous structure and they exist between the particles. The second type of pores called as intraparticle pores are within the particles since the particles are permeable. Furthermore, three types of porosities can be defined for a dual scale porous media as interparticle, intraparticle and bulk porosities. These porosities can be found by using following equalities:

$$\varepsilon_p = \frac{V_{vp}}{V_p}; \varepsilon_f = \frac{V_{vf}}{V_t}; \varepsilon_t = \frac{V_{vt}}{V_t} \quad (1.1)$$

where ε_f , ε_p and ε_t are the interparticle, intraparticle and bulk porosities, respectively. The volumes of interparticle, intraparticle and total pores are shown by V_{vf} , V_{vp} and V_{vt} , respectively. Furthermore, V_p and V_t are the total volumes of solid phase and dual scale porous media. The size of interparticle pores is generally greater than the intraparticle pores and consequently the interparticle porosity is generally greater than the intraparticle porosity. The inter- and intraparticle pores are also called as macro and micro pores by some researchers (Yu and Cheng, 2002). The fluid flow in a dual scale porous medium can also be classified into two types as inter- and intraparticle flows. Hence three related permeabilities can also be defined for a dual scale porous medium as interparticle, intraparticle and bulk permeabilities relating to flow in particle, between particle and the entire dual scale porous medium.

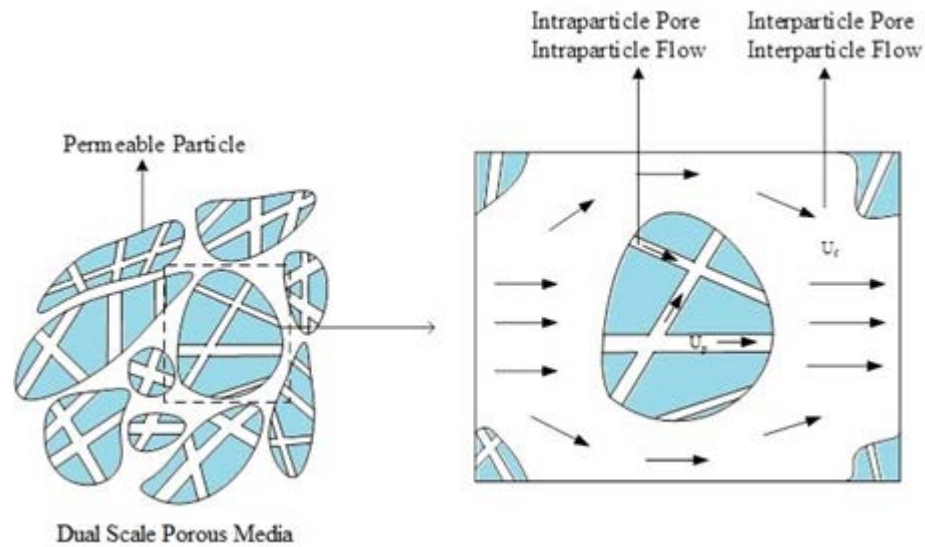


Figure 1.1. Schematic view of dual scale porous media

The application of dual scale porous media is widely faced in daily life, nature and industry. The flowing of a fluid through a fiber mat, woven fiber bundles, multifilament textile fibers, oil filters and fractured porous media are some examples for the application of the fluid flow through a dual scale porous media.

1.2. The Aim of Study

The aim of the present study is to investigate the effects of intraparticle porosity on the fluid flow and heat transfer in porous media containing inline array of square rods. The volume averaging method is used to determine the macroscopic transport parameters such as permeability and interfacial convective heat transfer coefficients. The Kozeny constant was determined by proposing a new correlation based on Kozeny-Carman permeability equation for the considered medium.

It should be mentioned that, most of studies on dual scale porous media were performed on porous media consist of permeable particles containing large number of intraparticle pores. However, there are applications (such as cracked rocks) in which limited number of intraparticle pores exist. Hence, the application of Darcy or Darcy-Brinkman equation for intraparticle flow is not correct. For those applications, fluid motion in the intraparticle pores should be solved by Stokes or Navier-Stokes equations. For the permeable particle with limited number of pore, the direction of the intraparticle pores takes important role in determination of permeability. In this study, a two

dimensional porous media consists of permeable square rods in inline arrangement is considered. Each particle in the porous media is splitted by two channels symmetrically and fluid can flow throughout these channels. The Navier-Stokes and Energy equations are solved for a representative elementary volume (REV) of the porous media and the velocity, pressure and temperature distributions for inter and intraparticle voids are found. Based on the obtained results, the intrinsic interparticle permeability (without considering intraparticle flow), intrinsic intraparticle permeability (without considering interparticle flow), bulk permeability and interfacial convective heat transfer coefficient are found. Two relations for determination of bulk permeability tensor in terms of intrinsic inter and intraparticle permeabilities are suggested. To the best of our knowledge, the results of the present study are new and motivate researchers to perform further pore level studies on porous media with cracked particles to develop relationships for determination of bulk permeability.

In the next section a wide literature survey on the determination of macroscopic transport parameters, microscopic and macroscopic governing equations and boundary conditions and computation procedure are presented in details.

1.3. Literature Review

A literature review on the determination of the macroscopic transport properties of porous media is presented. By using numerical methods, macroscopic transport properties such as permeability and interfacial convective heat transfer coefficient can be found theoretically. In this section the studies on determination of the permeability, Kozeny constant and interfacial heat transfer are reviewed. For all researches evaluate in this chapter, the aim of studies and assumptions made in the studies are shortly introduced. The tables are constructed to show some parameters of the studies such as proposed correlations and schematic view of the considered domain.

1.3.1. Literature Review on Permeability for Dual Scale Porous Media

In this section, the literature studies on determination of permeability in dual scale porous media are reviewed. Table 1.1 summarizes some pore level computational studies performed on fluid flow thorough a dual scale porous media. In the first column, the name of researcher and related reference number are given. In the second column, the governing equations solved to find velocity and pressure distributions for inter and intraparticle pores are written. The suggested correlation for the bulk permeability is given in third column. Finally, the schematic figure of the considered dual scale porous media is represented in the last column.

As can be seen from Table 1.1, most of performed studies relates to the porous media with permeable particles containing large number of intraparticle pores. That's why some researchers preferred to solve the Darcy or Brinkman equation to find velocity and pressure distribution for the permeable particle. Some researchers used Stokes or Navier-Stokes equation to find velocity and pressure fields in the permeable particles. An overview on the Table 1.1 shows that Papathanasiou (Papathanasiou, 2001), Hwang et. al. (Hwang and Advani, 2010), Byon and Kim (Byon and Kim, 2013), Yu and Cheng (Yu and Cheng, 2002), Nield and Kuznetsov (Nield and Kuznetsov, 2011) suggested correlations for determination of the bulk permeabilities by using experimental or theoretical methods.

The resistance that microstructure of fiber reinforcement creates on the fluid flow can be characterized by the permeability which is the ratio between the superficial velocity and pressure drop in the porous medium. As results of this condition, Ranganathan (Ranganathan, 1996) developed a predictive semi-analytical solution for flow across arrays of aligned cylinders with elliptical cross sections modeling the fiber mats. The out coming results of the permeability from the model were compared with numerical results obtained from finite element calculations over a range of volume fractions, cross-sectional shapes, and tow permeabilities. The flow through the porous region was solved by utilizing Brinkman's equation and the flow in the open region using Stokes' equation for fiber volume fractions of 0.70 and 0.80 the influence of the tow permeability on the overall permeability was investigated. The good agreement between the predicted and the numerical result were determined. It was found that the nominal

fiber volume fraction effect the overall tow permeability. The impact of the intra-tow flow increases as the nominal fiber volume fraction increases.

Ngo and Tamma (Ngo and Tamma, 2001) developed the concept of using a three-dimensional unit cell to predict permeability. The continuity equation and the creeping motion Stokes equation were solved to analyze the flow in the open or fluid region of the unit cell. In the intra-tow area where the tow consists of groups of fibers and can be treated as a porous medium, the flow is governed by the continuity equation and the Brinkman equation. The applied boundary conditions are constant pressure gradient over two opposing surfaces to drive the flow and symmetric conditions of pressure and velocity on the remaining surfaces of the unit cell. In the intra-tow (i.e., fiber tow) region, the equations derived by Gebart were used to find the permeability of the porous medium. The encouraging results were found for their predicted models.

Nedanov and Advani (Nedanov and Advani, 2002) predict the permeability of anisotropic fibrous porous media by using homogenization method to formulate governing equations and boundary conditions. In a periodic cell the permeability components were calculated by solving a boundary value problem. The application of the method was shown on a periodic cell modeling the geometry of woven fiber performs used in composites manufacturing. The resulting equations were solved using CFD package FIDAP. The effect of dual porosity and nesting of adjacent fabric layers on the macro permeability was investigated and the results were compared with experiments.

For dual scale fibrous structure Tahir et al. (Tahir et al., 2014) used the computational fluid dynamics methods to investigate the impact of different parameters on the overall permeability. Two models were developed for calculation of permeability one was resolved and the other one was homogenized porosity model. These models were compared with each other and good agreement is observed between the results of two numerical models. It was demonstrated that the effect of intra-tow porosity greater than 0.5 on the overall permeability is irrelevant, while the inter-tow porosity on the other hand has a very important effect on the overall permeability.

Full 3-D geometry of an idealized multifilament woven fabric were studied in the work of Wang et al. (Wang et al., 2006). The filaments were packed in hexagonal arrangement to find permeability. The comparison with the homogeneous anisotropic lumped model of Gebart was proposed where a satisfying agreement was obtained. However their results show that Gebart's model considered permeability of multifilament fabrics even at high yarn's solid volume fractions as an unimportant parameter.

Papathanasiou (Papathanasiou, 2001) performed a computational study by utilizing boundary element method to investigate the effect of viscous flow across unidirectional arrays of fiber bundles. The flow through the unit cell was solved by using numerical methods to compute the hydraulic permeability (K_p) of the dual porosity fibrous medium. The K_p values were determined through a large number of simulations for a range of inter- and intra-tow porosities. In that study they proposed a semi-empirical correlation for hexagonal and square intra-tow fiber arrangements to predict the permeability of fiber bundles which depends on inter and intra-tow porosities (i.e. inter and intra particle porosities), the type of intra-tow packing and the size (or number) of the intra-tow filaments.

Hwang et al. (Hwang and Advani, 2010) presented a new finite-element scheme to solve the Stokes–Brinkman equation for flow analyses in dual scale porous media. Based on numerical and analytic results they also proposed a simple relationship between the effective permeability and the permeability of fiber tow. Such a simple demonstrating indicated great adjustment with numerical results for an extensive range of the tow permeability on the condition that the tow permeability is small enough. In addition, they observed that geometrical arrangement of tows can dramatically influence the effective permeability in the unit cell. In addition

Nobovati et al. (Nobovati et al., 2010) used the lattice Boltzmann method to investigate the dual-scale problem of fluid flow through three-dimensional multifilament woven fabrics. In their study the inter-yarn porosity ('weave porosity', ϕ_w) and the intra-yarn porosity ('yarn porosity', ϕ_y) are changed in the range of $0.35 < \phi_w < 0.65$ and $0 < \phi_y < 0.8$, respectively. The weave and yarn permeabilities values (K_w and K_y) are dependent on these parameters. They discussed the effect of inter- and intra-yarn porosity on the effective permeability of the fabric, K_p , in terms of the fabric structure. They used the semi-empirical relationship between the fabric permeability and the weave and yarn permeabilities which was developed by Papathanassiou for two-dimensional structures. Their three dimensional simulations results provides an excellent fit with only minor adjustment fitting parameters.

Tung et al. (Tung et al., 2002) studied the effects of woven structures on fluid flow through the basic weaves of multifilament woven filter cloths numerically by using the FLUENT software. The flow pattern and the resistance to flow in the interstices were obtained by using numerical methods. The Results show that the construction of the fabric

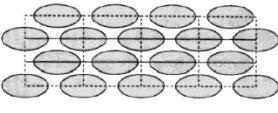
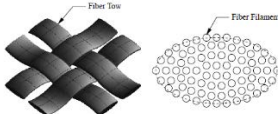
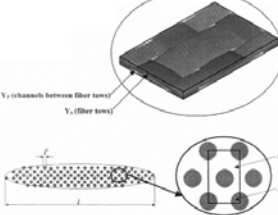
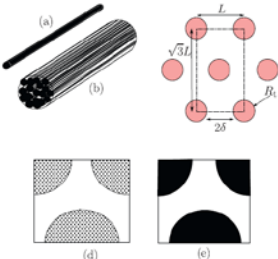
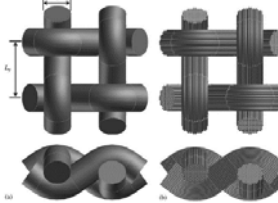
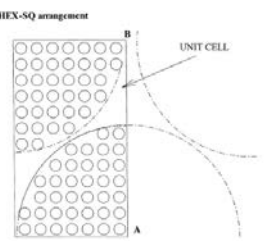
pores has an important effects on the flow pattern in the interstices and the downstream. Moreover, in the case of tightly woven filter cloths, the main flow passes through the yarns of the cloth; while the direction of flow is generally around the yarns of a loosely woven cloth.

Nield and Kuznetsov (Nield and Kuznetsov, 2011) obtained analytical solution in a channel occupied by a bidisperse (dual scale) porous medium. The relations suggested by them contain three permeabilities as interparticle, intraparticle and bulk permeabilities. The interaction between inter- and intraparticle velocities which causes an extra pressure drop through the dual scale porous media is included by an extra term contains a coefficient (ζ) called as velocity coupling coefficient.

Byon and Kim (Byon and Kim, 2013) analyzed the permeability of bidispersed (dual scale) and mono dispersed porous media both with experimental and analytical methods. The effect of particle size distribution and the packing structure of particle on the permeability was investigated separately. To construct the bi-dispersed porous media, the mono-dispersed porous medium is grinded into clusters, sieved into specific sizes and sintered again. In their studies inter and intraparticle sizes were chosen as 650 and 117 μm respectively. A term involving mean particle diameter and mean cluster size was multiplied to Blake-Kozeny equation to satisfy the obtained numerical and experimental results. Their results predicted that the permeability of the bi-dispersed porous media quasi-linearly decreases as the range of cluster size increases, and almost independent of the particle size distribution.

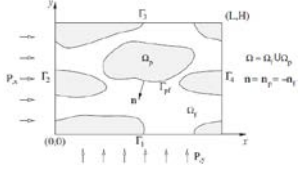
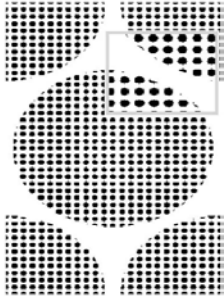
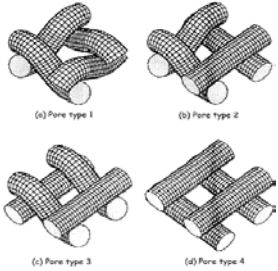
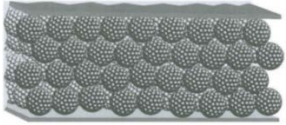
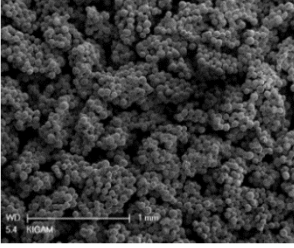
Yu and Cheng (Yu and Cheng, 2002) developed fractal permeability model for dual scale (bi-dispersed) porous media. Their model was based on fractal characteristics of pores in media and it was found that the model should be a function of the tortuosity fractal dimension, pore area fractal dimension, sizes of particles and clusters, micro-porosity inside clusters, and the effective porosity of a medium. In their study the micro porosity value was in the range of $0.093 < \phi_i < 0.215$. They found a good agreement between the fractal model prediction of permeability and experimental data.

Table 1.1. The performed studies and suggested relations for determination of permeability in a dual scale porous media

Study	Equations	Suggested correlation	
Ranganathan (1996)	Stokes equation for Interparticle Brinkman equation for Intraparticle	$K_{eff} = \frac{L}{H} \frac{1}{I}$ <p>Note: I is a long expression defined in the paper</p>	
Ngo and Tamma (2001)	Stokes equation for Interparticle, Brinkman equation for Intraparticle	-----	
Nedanov and Advani (2002)	Stokes equation for interparticle, Darcy's law for intraparticle	-----	
Tahir et al. (2014)	Navier Stokes equations for Inter and Intraparticle	-----	
Wang et al. (2006)	Navier Stokes equations for Inter and Intraparticle	-----	
Papathanasiou (2001)	Stokes equation for Inter and Intraparticle	$Y \equiv \frac{K_p K_s^{0.5}}{K_{tow}^{1.5}} = a \left(\frac{K_s}{K_{tow}} \right)^n \times \left(1 + \frac{1}{\alpha} \left(\frac{K_s}{K_{tow}} \right)^{1.5-n} \right)$ <p>Note: For hexagonal arrays of fiber bundles</p>	

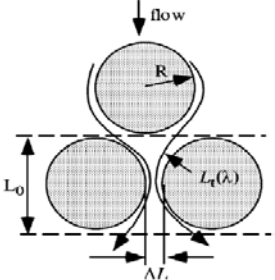
(cont. on next page)

Table 1.1. (cont.)

<p>Hwang and Advani (2010)</p>	<p>Stokes equation for Interparticle, Brinkman equation for Intraparticle</p>	$K \approx C_{pressure} + C_{slip} \sqrt{K_p}$ <p>Note: $C_{pressure}$ and C_{slip} are given in paper</p>	
<p>Nabovati et al. (2010)</p>	<p>LBM for Inter and Intraparticle</p>	<p>-----</p>	
<p>Tung et. al. (2002)</p>	<p>Navier Stokes equations for Interparticle, Darcy's Law for Intraparticle</p>		
<p>Nield and Kuznetsov (2011)</p>	<p>Theory was developed</p>	$K = \frac{1}{1 + (\zeta / \mu)(K_f + K_p)} \times (\phi K_f + (1 - \phi)K_p + 2(\zeta / \mu)K_f K_p)$	
<p>Byon and Kim (2013)</p>	<p>Navier Stokes equations for Interparticle, Darcy's Law for Intraparticle</p>	$K_{bi} = \frac{\varepsilon^3 D_c^2}{150(1 - \varepsilon)^2} \left[1 + 4.03 \exp \left(3.29 \frac{D_p}{D_c} \right) \left(\frac{D_p}{D_c} \right)^2 \right]$	

(cont. on next page)

Table 1.1. (cont.)

<p style="text-align: center;">Yu and Cheng (2002)</p>	<p style="text-align: center;">Fractured model theory</p>	$K = \frac{\pi}{128} \frac{L_0^{1-D_f}}{A} \times \frac{D_f}{3 + D_f - D_f} \lambda_{\max}^{-3+D_f}$	
--	---	--	---

1.3.2. Literature Review on Kozeny Constant

To determine the permeability the Kozeny constant is used. Since these two parameters are related to each other, Kozeny constant can be found by using Kozeny-Carman equation. In this section, the literature studies on determination of Kozeny constant are presented. The summary of the studies and suggested correlations are displayed in Table 1.2.

Singh and Mohanty (Singh and Mohanty, 2000) studied the effects of porosity on the permeability of 3D porous media by using lattice-Boltzmann method. Carman-Kozeny equation was employed to determine the permeability in which the Kozeny constant is declared as function of the correlation length. The modified-Kozeny constant was found to decrease with increasing correlation length for low correlation lengths; however, it was found to be nearly constant for higher correlation lengths.

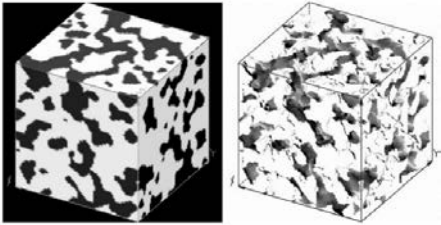
Xu and Yu (Xu and Yu, 2008) extract new analytical expression for the permeability and Kozeny constant in the homogeneous porous media based on the fractal geometry theory. The predicted Kozeny constant was employed as a function of the fractal dimensions and porosity. A correlation that relates permeability with porosity and the geometrical dimensions of fractal medium was proposed. It was found that the Kozeny constant model based on fractal theory is more effective in determining the permeability than the traditional methods and models. Furthermore, it was mentioned that the Kozeny constant is actually not a constant and depends strongly on porosity and the microstructures of pores and capillaries.

Teruel and Rizwan-uddin (Teruel and Rizwan, 2009) studied a representative elementary volume of a porous medium containing square cylinders of staggered arrangement. Reynolds numbers between 10^{-3} and 10^5 were considered and porosities

between 0.05 and 0.95 were simulated for each Reynolds number. The change of permeability with porosity was investigated and the comparison with Carman- Kozeny equation was made. The numerical data obtained in the study were used to propose a new correlation for the permeability of the medium as a function of porosity. They claimed that this correlation is valid over the entire range of considered porosity (5–95%) better than the Carman–Kozeny equation

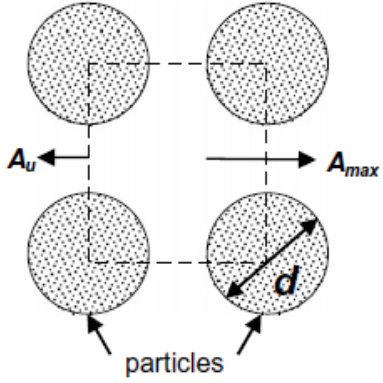
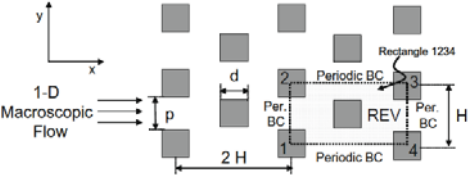
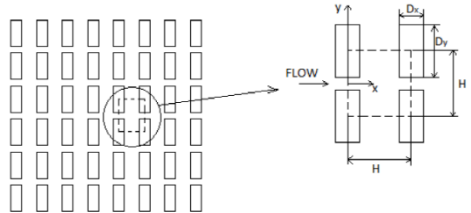
In Ozgumus et al. (Ozgumus et al., 2014) study, the permeabilities of porous media that contains rectangular rods are solved, numerically. The relevance of Kozeny-Carman equation for the periodic porous media is examined and the influence of porosity and pore to throat size ratio on Kozeny constant were studied. For a specific porous medium the suggestion of a fixed value for Kozeny constant makes the utilization of Kozeny-Carman permeability equation too limited. In their research, they claimed that the Kozeny constant cannot depend just on porosity and the effect of pore to throat size ratio (i.e. β) should be considered to enhance the applicability of Kozeny-Carman equation for wide scope of the geometrical parameters. Moreover, an equation for Kozeny constant in terms of porosity and pore to throat size ratio is suggested for the studied periodic structure. The proposed equation gives precise results for the determination of the permeability for porosity range from 0.2 to 0.9 and pore to throat size ratio values from 1.63 to 7.46.

Table 1.2. Theoretical studies on the determination of Kozeny constant

study	Suggested Correlations	
Singh and Mohanty (2000)	-	

(cont. on next page)

Table 1.2. (cont.)

<p>Xu and Yu (2008)</p>	<p>-</p>	
<p>Teruel and Rizwanuddin (2009)</p>	<p>$k_K = 8.1875$ for $\varepsilon < 0.55$</p>	
<p>Ozgumus et al. (2014)</p>	<p>$k_K = A\varepsilon^B$ for $\left\{ \begin{array}{l} 0.2 < \varepsilon < 0.9 \\ 1.63 < \beta < 7.46 \end{array} \right\}$ $A = C_0\beta^4 + C_1\beta^3 + C_2\beta^2 + C_3\beta + C_4$ $B = D_0\beta^4 + D_1\beta^3 + D_2\beta^2 + D_3\beta + D_4$ Note: C_x and D_x values are given in the paper</p>	

1.3.3. Literature Review on Interfacial Convective Heat Transfer Coefficient

In this section, the literature survey of interfacial convective heat transfer coefficient are reviewed. The reviewed studies are summarized in Table 1.3. In this table the correlations found to determine the interfacial Nusselt number are shown.

Square rods are studied by Kuwahara et al. (Kuwahara et al., 2000) in staggered arrangement to determine the interfacial convective heat transfer coefficient. The rods are taken into an isothermal environment at a constant temperature, which was different than

the film temperature of the fluid. Periodicity of the problem cause to take a single structural unit into consideration. The Reynolds number was varied from 0.01 to 1000 and the porosity from 0.36 to 0.96. Prandtl number is in between 0.01 to 100. For the wide range of porosities iterative computations are done to obtain proper correlations for interfacial Nusselt number. As a result, the predictions of correlations are consistent with the experimental data in the literature.

Nakayama et al. (Nakayama et al., 2002) has examined numerical experiments on pore scale by the use of full set of Navier stokes and energy equations to simulate laminar fluid flow and heat transfer through an anisotropic porous medium. Temperature of the rods was chosen as to be constant and different than the temperature of the following fluid. Boundary conditions at the inlet and outlet were the periodic boundary conditions. In the longitudinal flow it is observed that the interfacial Nusselt number does not change very much with Reynolds number. However, there is slight drop in Nusselt number near $Re = 10$. A correlation was proposed for the Nusselt number with the correlation coefficients that depend on the degree of the anisotropy of the medium and the flow direction. It is observed that the coefficients decrease with increasing anisotropy degree.

According to Saito and de Lemos (Saito and de Lemos, 2006), the experimental analysis was conducted on an infinite porous medium in which fully-developed flow condition occurs. Laminar flow conditions were considered for particle based Reynolds number range of 4 to 400 and porosity range of 0.44 to 0.9. In one of the surveys, square rods were in staggered arrangement and the rods were assumed isothermal. In addition they determined the interfacial convective heat transfer coefficient for the turbulent flow regime in the same porous medium. High and low Reynolds $k-\epsilon$ turbulence models were used in conjunction of a two-energy equation model. A correlation is proposed for the interfacial Nusselt number in terms of porosity, Reynolds and Prandtl numbers for the Reynolds numbers between 104 and 107.

For low Reynolds number flows ($0.05 < Re < 40$), Gamrat et al. (Gamrat et al., 2008) was studied the determination of interfacial Nusselt numbers of banks of square rods in inline and staggered arrangements. Both constant wall temperature and constant volumetric heat source were considered as thermal boundary conditions. Peclet numbers between 0.01 and 1000 and Prandtl numbers between 1 and 100 were assumed. After the survey, the results show that the heat transfer in the array of rods was insensitive to thermal boundary condition at the interface for the highest values of Reynolds and Prandtl numbers and porosity. It was examined that the Nusselt number was more influenced by

the enhanced convective effect for the staggered arrangement. Also it is observed that for small porosity values, the heat transfer performance was slightly higher for the staggered arrangement especially. Nusselt correlations were done both for the aligned and staggered arrangements by the suggestion of the article (Gamrat et al.). To conclude, the heat transfer between the solid and fluid phases in the thermal non-equilibrium condition was observed to be affected by the thermal boundary condition used for the solid phase.

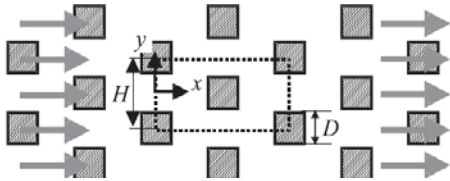
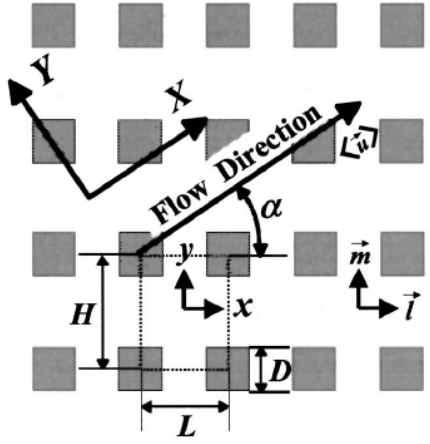
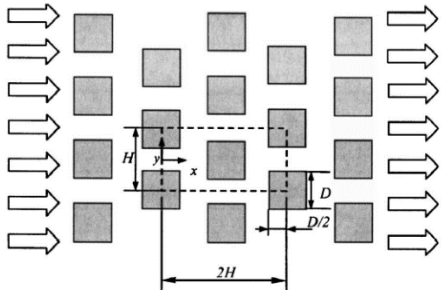
The effects of the representative elementary volume (REV) aspect ratio is investigated in Alshare et al. (Alshare et al., 2010) for macroscopic flow direction and Reynolds number on the interfacial convective heat transfer coefficient for the inline arrangement of square rods. In this study, temperature boundary condition is chosen as constant heat flux at the interfaces. For periodic array of square rods, variation of the interfacial Nusselt number with Reynolds number for different structural unit aspect ratios is observed. The interfacial convective heat transfer coefficient does not show too much change with Reynolds number for flow in the longitudinal direction. However, for flow in the direction with 45o angle, Reynolds number showed increase. In addition, the heat transfer coefficients were found to have minimal values, for the flow along the principal axes.

Macroscopic transport parameters through the square rods for both inline and staggered arrangements for a fully developed flow were investigated by Lopez Penha et al. (Lopez Penha et al., 2012). A volumetric heat generation in the rods was considered to be constant for the various solid-to-fluid thermal conductivity ratios and Reynolds numbers. Periodic representative elementary volumes of the porous media were selected and a finite volume based algorithm was used to solve the governing equations. Their results indicated that for solid-to-fluid thermal conductivity ratios higher than 100 the interfacial Nusselt number is almost constant since it changes significantly for lower values. It was specified that as thermal conductivities reach the same order of magnitude, the temperature gradients across the interface decline and subsequently, Nu value reduce with decreasing solid-to-fluid thermal conductivity ratio.

Ozgumus and Mobedi (Ozgumus and Mobedi, 2014) investigate the effects of pore to throat size ratio on the interfacial heat transfer coefficient for a periodic porous media containing inline array of rectangular rods numerically. The study is performed for pore to throat size ratios between 1.63 and 7.46, porosities from 0.7 to 0.9, and Reynolds numbers between 1 and 100. It is observed that in addition to porosity and Reynolds number, the parameter of pore to throat size ratio plays an important role on the heat

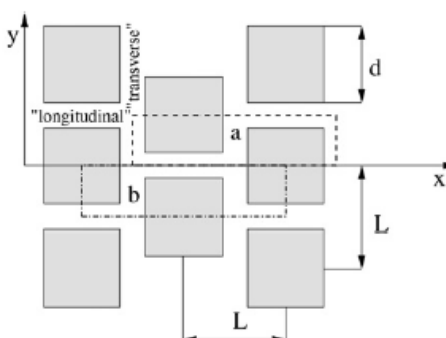
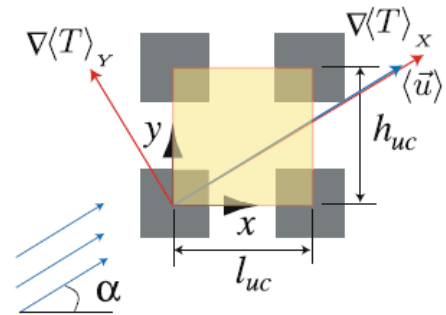
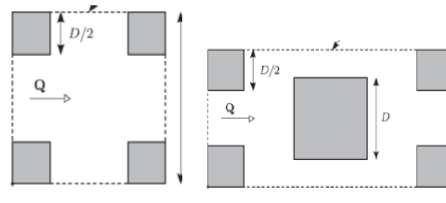
transfer in porous media. For the low values of pore to throat size ratios ($\beta = 1.63$), Nusselt number increases with porosity while for the high values of pore to throat size ratios ($\beta = 7.46$), the inverse conduct is observed. In the light of numerical results, a correlation for the determination of Nusselt number in terms of porosity, pore to throat size ratio, Reynolds and Prandtl numbers is proposed.

Table 1.3. Theoretical studies on the determination of interfacial convective heat transfer coefficient

Study	Suggested Correlations	
Kuwahara et al. (2001)	$Nu_D = \left(1 + \frac{4(1-\varepsilon)}{\varepsilon}\right) + \frac{1}{2}(1-\varepsilon)^{1/2} Re_D^{0.6} Pr^{1/3}$ $\left. \begin{aligned} 10^{-2} \leq Re \leq 10^3 \\ 10^{-2} \leq Pr \leq 10^2 \\ 0.36 \leq \varepsilon \leq 0.96 \end{aligned} \right\}$	
Nakayama et al. (2002)	$Nu_D = \frac{1}{2} \left(c_{f1} \cos^2 \alpha + c_{f2} \sin^2 \alpha \right) + \frac{d_{f1}^{0.3}}{2^{0.4}} Re_D^{0.6} Pr_f^{1/3}$ $\left. \begin{aligned} 10^{-2} \leq Re \leq 10^3 \\ Pr = 1 \\ \varepsilon = 0.75, 0.833, 0.875 \end{aligned} \right\}$ <p>Note: α is flow angle, c_x and d_x values are given in the paper</p>	
Saito and de Lemos (2006)	$Nu_D = 0.08 \left(\frac{Re_D}{\varepsilon} \right)^{0.8} Pr^{1/3}$ $\left. \begin{aligned} 10^4 < \frac{Re_D}{\varepsilon} < 2 \times 10^7 \\ 0.2 < \varepsilon < 0.9 \end{aligned} \right\}$	

(cont. on next page)

Table 1.3. (cont.)

<p>Gamrat et al. (2008)</p>	<p>For inline arrangement:</p> $Nu_D = 3.02(1 - \varepsilon)^{0.278} \exp[2.54(1 - \varepsilon)] + [0.44(1 - \varepsilon) + 0.092] Re_D^{0.5} Pr^{0.2}$ <p>For staggered arrangement:</p> $Nu_D = 3.02(1 - \varepsilon)^{0.278} \exp[2.54(1 - \varepsilon)] + [1.093(1 - \varepsilon) + 0.357] Re_D^{0.5} Pr^{0.2}$ $\left\{ \begin{array}{l} 0.05 \leq Re_D \leq 40 \\ 1 \leq Pr \leq 100 \\ 0.44 \leq \varepsilon \leq 0.98 \end{array} \right\}$	
<p>Alshare et al. (2010)</p>	$\left\{ \begin{array}{l} 1 \leq Re \leq 1000 \\ \varepsilon = 0.75 \text{ and } 0.875 \end{array} \right\}$ <p>Graphical Presentation</p>	
<p>Lopez Penha et al. (2012)</p>	$\left\{ \begin{array}{l} 0.01 \leq Re \leq 200 \\ \varepsilon = 0.75 \\ Pr = 1 \\ 1 \leq k_s/k_f \leq 104 \end{array} \right\}$ <p>Graphical Presentation</p>	
<p>Ozgumus et al. (2014)</p>	$Nu = (a_0\varepsilon + a_1) + (a_2\varepsilon + a_3) Re^{0.6} Pr^{1/3}$ $a_i = a_{i1} + a_{i2}\beta + a_{i3}\beta^2$ <p>Note: a_{xx} values are given in the paper</p> $\left\{ \begin{array}{l} 1 \leq Re \leq 100 \\ 0.7 < \varepsilon < 0.9 \\ 1.63 < \beta < 7.46 \end{array} \right\}$	<p>Same with Ozgumus et al. 2014 (Table 1.2)</p>

1.4. The Outline of Thesis

The thesis is divided into six chapters. The first chapter includes an introduction to the dual scale porous media, the aim of study and detail literature review on the determinations of permeability in dual scale porous media, Kozeny constant and interfacial convective heat transfer

In Chapter 2, fundamental concepts of porous media and background of microscopic and macroscopic methods are given. Microscopic governing equations for fluid flow and heat transfer and macroscopic equations are presented. The derivation of the macroscopic fluid flow and heat transfer equations with mathematical definitions of permeability and interfacial convective heat transfer coefficient are exhibited.

Chapter 3 comprises the considered domain with the geometrical properties of the studied porous media is presented. The governing equations solved to obtain the microscopic velocity, pressure and temperature distributions in the REV's and the corresponding boundary conditions for calculation of the macroscopic transport parameters are clarified in detail.

In chapter 4 the numerical procedure employed in the determination of the permeability and interfacial convective heat transfer coefficient are demonstrated. Computational details and grid independency tests of the computations are given in this chapter as well.

Chapter 5 contains the results for the present study. The detail explanations of graphics and figures in advanced. The proposed correlations for Kozeny constant and the discussions about interfacial convective heat transfer coefficient are also reported in this chapter. Finally, by taking into account of predicted results the concluded remarks submitted in Chapter 6.

CHAPTER 2

FUNDAMENTALS OF MACROSCOPIC HEAT AND FLUID FLOW ANALYSIS IN POROUS MEDIA

A porous medium is called as a composite medium consists of voids and solid particles inside. The behavior of the stream passing through these pores is complex where the three dimensional flow is observed. For this reason the pore level determination of velocity and temperature distributions is troublesome and difficult. To overcome these challenges more proper approaches are obliged in analyzing the heat and fluid flow in porous media. The most widely recognized techniques is the macroscopic approach which is clarified in this chapter.

In this section, the microscopic and macroscopic methods for investigating fluid flow and heat transfer in the porous media are presented. Firstly, an introduction to the microscopic point of view and the microscopic concepts of porous media are exhibited. At that point, the microscopic fluid flow and heat transfer equations are introduced and explained. At last, the macroscopic equations are presented and the determination of general forms of macroscopic momentum and energy equations are clarified in point of interest.

2.1. Microscopic and Macroscopic Views of Porous Media

The fluid in a porous medium flows in the pores (or voids) between the particles. An open porous medium has interconnected voids and solid particles; subsequently the fluid flows in the voids. If there may be periodicity in the porous structure, those medium is called as ordered or structured. In the event that the structure is irregular or randomly oriented, it is named as disordered (unstructured) porous medium (see Figure 2.1). Disordered (randomly) packed beds are widely utilized in industrial processes, because of their low cost and facilitate of packing. But, pressure drops in these packed beds are conventionally much higher with respect to the ordered packed beds. The overall heat transfer performances of this type of porous media is also poor which made ordered

packed beds to be considered as a promising choices for the industrial applications (Yang et al., 2010).

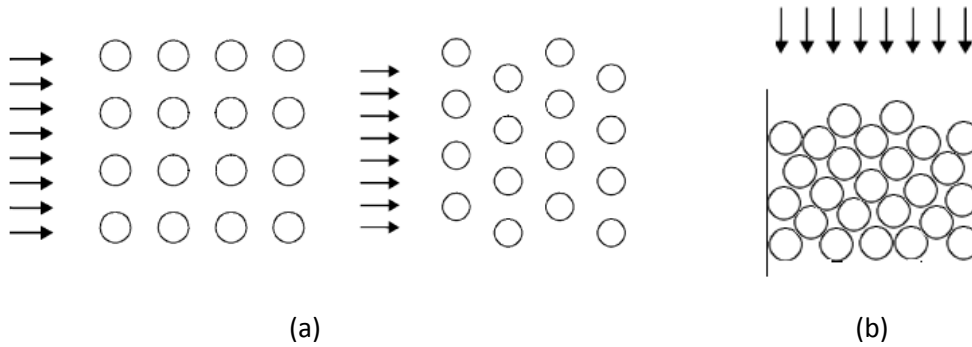


Figure 2.1. Schematic views of porous media (a) ordered, (b) disordered porous media

Porosity is the fundamental property concept in a porous media. It is defined as the volume of the voids to the total volume of the porous media (see equation (2.1)).

$$\varepsilon = \frac{V_f}{V} \quad (2.1)$$

where V_f is the volume of the pores in the porous medium and V is the total volume.

As specified before, there are predominantly two approaches to deal with heat and fluid flow in porous media: microscopic and macroscopic approaches. Fluid kinetics and motions in pores between particles is studied as it is in the microscopic approach. The continuity and Navier-Stokes equations are used in this kind of study however it is hard and difficult to dissect the heat and fluid flow for entire domain of a porous medium, microscopically. The microscopic approach is helpful when a periodic structure is considered.

As another point of view, in the macroscopic approach, heat and fluid flow is analyzed for a continuum domain by upscaling the microscopic parameters. Heat and fluid flow equations are set up for a continuum space including the whole volume of porous medium in spite of discontinuity in the flow due to the solid phase and all properties of the domain are obtained as effective values. Volume integral of the continuity, momentum and energy equations yields the governing equations for the entire of porous medium.

Figure 2.2 reveals fluid flow in a channel occupied with a porous medium. At the point when fluid goes into the channel, fluid particles have 3D movements inside the pores. Anyhow macroscopically, flow through the porous column is unidirectional and the macroscopic velocity can be composed as the ratio of volume flow rate to the cross-sectional area. This macroscopic velocity is otherwise called apparent, superficial or Darcian velocity. This velocity should be constant through channel due to the conservation of mass (Nakayama, 1995).

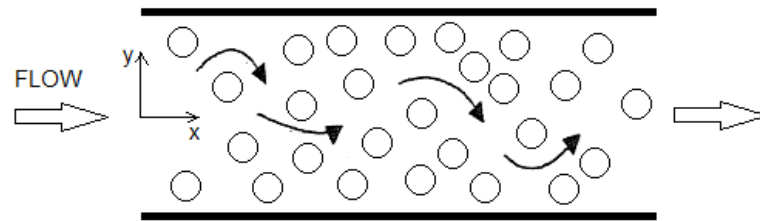


Figure 2.2. Macroscopic and microscopic flows through a porous channel.

Permeability is a macroscopic transport property used to obtain macroscopic velocity. Permeability is a quantification of the allowance fluid flow through the solid structure. It is independent of fluid properties and just relies on upon properties of the solid structure of the considered porous medium (Nield and Bejan, 2006).

Additionally the investigation of heat transfer in porous media is carried out by using macroscopic method. Interfacial convective heat transfer transport is an essential parameter that plays important role on analyzing heat transfer in porous media.

Interfacial convective heat transfer coefficient represents the heat transfer between fluid and solid phases. It happens when there is no local thermal equilibrium between two phases. For study of the interfacial convective heat transfer coefficient two phases in the porous medium should be considered, independently. Two energy equations (one for solid and another for fluid phase) should be solved to determine temperature field for the entire domain.

2.2. Microscopic Fluid Flow and Energy Equations

For an incompressible flow of Newtonian fluid with constant thermo-physical properties, the continuity and momentum equations, given in equations (2.2) and (2.3),

are utilized to acquire the velocity and pressure distributions in the pores of the considered porous medium.

$$\nabla \cdot \vec{u} = 0 \quad (2.2)$$

$$\rho_f \frac{\partial \vec{u}}{\partial t} + \rho_f (\vec{u} + \nabla \vec{u}) = -\nabla p + \mu_f \nabla^2 \vec{u} \quad (2.3)$$

Where \vec{u} is the velocity vector, ρ_f and μ_f are the density and dynamic viscosity of the fluid, respectively, and p is pressure. In a porous medium to obtain the microscopic temperature distribution, solid phase as well as fluid phase should be considered discretely and two microscopic energy equations may be taken into account. The individual form of microscopic energy equations for fluid and solid phases is given in equations (2.4) and (2.5) respectively. If the negligible viscous dissipation is assumed

$$\rho_f c_{pf} \left(\frac{\partial T_f}{\partial t} + \nabla \cdot \vec{u} T_f \right) = k_f \nabla^2 T_f \quad (2.4)$$

$$\rho_s c_{ps} \frac{\partial T_s}{\partial t} = k_s \nabla^2 T_s \quad (2.5)$$

where T is temperature, c_p and k are specific heat capacity and thermal conductivity, respectively. The subscripts f and s refer to the fluid and solid phases. By using above governing equations (equations (2.2)-(2.5)) with appropriate initial and boundary conditions, the velocity and pressure distributions in the pores and the temperature distributions in both solid and fluid phases can be obtained. However, for a porous medium comprising of large number of pores and complex structure, the microscopic (or pore level) examination by utilizing these equations may be troublesome and time consuming. That is the reason; the macroscopic method which is clarified in the accompanying segments can be utilized to analysis fluid flow and heat transfer in porous media.

2.3. Volume Averaging Method

Analysis of heat and fluid flow in porous media is frequently performed by using volume averaging technique.

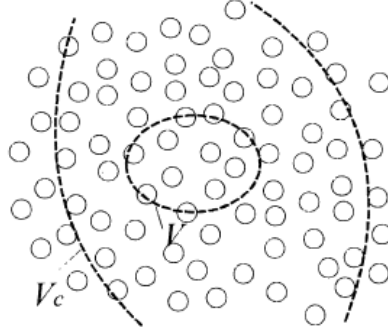


Figure 2.3. Microscopic control volume in a porous structure (Nakayama, 1995)

Volume averaging of a quantity over a control volume is computed as follows:

$$\langle \phi \rangle = \frac{1}{V} \int_V \phi dV \quad (2.6)$$

where V is the volume of chosen control volume. By using equation (2.6), the macroscopic velocity is defined as below.

$$\langle \bar{u} \rangle = \frac{1}{V} \int_V \bar{u} dV \quad (2.7)$$

In the event that an average value of a quantity for one of the phases is required, intrinsic averaging is used. For instance, the average velocity in the fluid phase can be calculated from equation (2.8). This velocity can likewise be called as pore or interstitial velocity and it is corresponding to the macroscopic velocity.

$$\langle \bar{u} \rangle^f = \frac{1}{V_f} \int_{V_f} \bar{u} dV \quad (2.8)$$

where V_f is pore volume.

More points of interest on the basics and uses of volume averaging method can be found in the book of Whitaker (Whitaker, 1999).

2.4. Darcy and Forchheimer Motion Equations

In 1856 Darcy found that (Darcy, 1856) the macroscopic (Darcian) velocity through a section of porous medium is relative to the pressure gradient and inversely proportional to the fluid viscosity. This relation is called as Darcy's Law and its one-dimensional form is demonstrated by equation (2.9). The proportionality constant K is known as permeability and it refers to the flow resistance inside the porous medium. The permeability is a tensor in which the diagonal terms show the permeability of the porous medium in principal directions. It relies on the micro-structure of the solid phase and free of the properties of the fluid (Nakayama, 1995). Darcy's Law is valid for low Reynolds number flows and can be accurately used to obtain average velocity in a porous medium for ($Re_d < 1$, $Re_d = \langle u \rangle d / \nu$) because it expresses a balance between viscous and pressure forces.

$$\langle u \rangle = \frac{K}{\mu_f} \left(\frac{d \langle p \rangle^f}{dx} \right) \quad (2.9)$$

An extra quadratic term which includes the flow inertia effects was proposed by Dupuit (Dupuit, 1863) and Forchheimer (Forchheimer, 1901), (Nakayama, 1995) for higher Reynolds number. The subsequent equation is called as Forchheimer extended Darcy's Law and its one dimensional form is provided by equation (2.10). The first term on the right hand side records for the frictional drag (Darcy term) and at the same time the second term (Forchheimer) refers to the drag.

$$-\frac{d \langle p \rangle^f}{dx} = \frac{\mu_f}{K} \langle u \rangle + \frac{C}{K^{1/2}} \rho_f (\langle u \rangle)^2 \quad (2.10)$$

where C is Forchheimer coefficient. In order to predict macroscopic velocity in a porous medium precisely as can be seen from equations (2.9) and (2.10), the permeability and Forchheimer coefficients values should be well known. The most

well-known mathematical expression for determination of permeability was derived according to Kozeny-Carman theory (Kozeny, 1927), (Carman, 1937). In the following passages the Kozeny-Carman theory and the derivation of Kozeny-Carman permeability equation are summarized. The average velocity for Hagen-Poiseuille flow in a channel with diameter of d_i can be found as:

$$\langle u \rangle^f = -\frac{1}{32\mu} \frac{d\langle p \rangle^f}{dx} d_i^2 \quad (2.11)$$

By using Dupuit-Forchheimer relation and comparing Darcy's Law with equation (2.11), the permeability value for Hagen-Poiseuille flow in a channel can be found as $K = d_i^2 \varepsilon / 32$.

As indicated in Figure 2.4 Kozeny considered the medium as a bundle of capillary channels with the same radius.

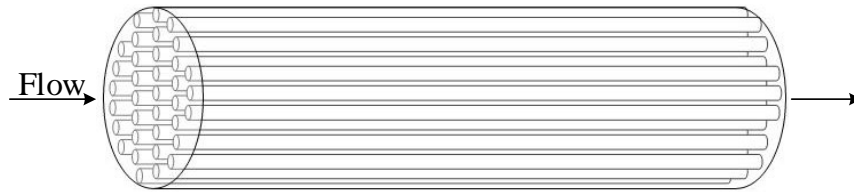


Figure 2.4. Flow through a bundle of capillary tubes

By combining Hagen-Poiseuille velocity equation with Darcy's Law and utilizing tortuosity idea, the accompanying equation for permeability was proposed by Kozeny:

$$K = \frac{d_i^2 \varepsilon}{32 \tau} \quad (2.12)$$

where τ is tortuosity. Tortuosity can be defined as the proportion of the actual length of flow path in the porous medium to the length of flow path in the absence of porous medium (i.e., in clear fluid). The impact of the microstructure of the porous medium (direction of the pores) on the macroscopic flow can be thought as tortuosity (Liu and Masliyah, 2005). Tortuosity used as a part of equation (2.12) may be defined as the correction to the pressure gradient which is characterized for clear fluid (Kaviany, 1995). The permeability equation of Kozeny was modified later by Carman and the so-called

Kozeny-Carman equation which predicts the permeability sensibly well for the packed bed of spheres is introduced as:

$$K = \frac{d_h^2 \varepsilon}{16k_K} \quad (2.13)$$

where d_h is the pore hydraulic diameter of the porous medium. The pore hydraulic diameter is defined as:

$$d_h = \frac{4\varepsilon}{A_0(1-\varepsilon)} \quad (2.14)$$

where A_0 is the ratio of the fluid-solid interfacial area to the solid volume. The symbol of k_K in equation (2.13) is Kozeny constant which includes the effects of flow path, particle shape and their connections (i.e., tortuosity and shape effects) and offer equivalent to a constant in Kozeny-Carman theory ($k_K = 5$). For spherical particles, the Kozeny- Carman equation can be revised in the light of particle diameter as equation (2.15).

$$K = \frac{1}{36k_K} \frac{\varepsilon^3}{(1-\varepsilon)^2} d^2 \quad (2.15)$$

where d is the diameter of the spheres. On the other side, for two or three dimensional cylinders equation (2.13) changes into equation (2.16).

$$K = \frac{1}{16k_K} \frac{\varepsilon^3}{(1-\varepsilon)^2} d^2 \quad (2.16)$$

where d is the diameter of the cylinders.

The macroscopic fluid flow equations are shortly clarified in the past passages. The conventional equations were for the most part acquired intuitionally by using experimental observations. However by applying volume averaging method on the relating microscopic equations, general forms of macroscopic fluid flow and heat transfer equations can be obtained theoretically. The macroscopic equations and the derivation procedure are exhibited in the accompanying sections.

2.5. General Forms of Macroscopic Motion Equations

By applying the volume averaging method on the continuity and Navier-Stokes equations general macroscopic flow equations can be acquired. To obtain intrinsic average of any multiplication $\varphi_1\varphi_2$ the following relationship can be used (Nield and Bejan, 2006).

$$\langle \varphi_1\varphi_2 \rangle^f = \langle \varphi_1 \rangle^f \langle \varphi_2 \rangle^f + \langle \varphi_1' \varphi_2' \rangle^f \quad (2.17)$$

Where the prime denotes the deviation of the intrinsic average value from the microscopic one, such that

$$\varphi' = \varphi - \langle \varphi \rangle^f \quad (2.18)$$

Equation (2.17) can be reworked regarding of the total volume averaged variables with using Dupuit-Forchheimer relation as follows.

$$\langle \varphi_1\varphi_2 \rangle = \frac{1}{\varepsilon} \langle \varphi_1 \rangle \langle \varphi_2 \rangle + \langle \varphi_1' \varphi_2' \rangle \quad (2.19)$$

Additionally, the following principles which are analogous to Leibnitz rule are used in the volume averaging procedure.

$$\langle \nabla \varphi \rangle = \nabla \langle \varphi \rangle + \frac{1}{V} \int_{A_{sf}} \varphi dA \quad (2.20)$$

$$\left\langle \frac{\partial \varphi}{\partial t} \right\rangle = \frac{\partial \langle \varphi \rangle}{\partial t} \quad (2.21)$$

where A_{sf} is the interfacial area between solid and fluid phases. By utilizing these equalities, macroscopic governing equations can be straightforwardly gotten from the microscopic equations. The macroscopic continuity equation can be obtained by applying volume averaging method to equation (2.2) which is the microscopic continuity equation.

$$\frac{1}{V} \int_V \nabla \cdot \vec{u} = \langle \nabla \cdot \vec{u} \rangle = 0 \quad (2.22)$$

The integration rule given by equation (2.20) is used on equation (2.20) to obtain equation (2.23).

$$\nabla \cdot \langle \vec{u} \rangle + \frac{1}{V} \int_{A_f} \vec{u} dA = 0 \quad (2.23)$$

The second term vanishes since the flow cannot enter through the solid wall. Henceforth the macroscopic continuity equation is found as follows.

$$\nabla \cdot \langle \vec{u} \rangle = 0 \quad (2.24)$$

The macroscopic momentum equation can also be found. With a similar procedure explained for obtaining macroscopic continuity equation, Volume averaging of microscopic momentum equation which is given by equation (2.3) yields:

$$\rho_f \left\langle \frac{\partial \vec{u}}{\partial t} \right\rangle + \rho_f \langle \vec{u} \cdot \nabla \vec{u} \rangle = -\langle \nabla p \rangle + \mu_f \langle \nabla^2 \vec{u} \rangle \quad (2.25)$$

This equation can be rewritten in the following form by using equations (2.20) and (2.21):

$$\begin{aligned} \rho_f \frac{\partial \langle \vec{u} \rangle}{\partial t} + \rho_f \left[\frac{1}{\varepsilon} \langle \vec{u} \rangle \cdot \nabla \langle \vec{u} \rangle + \langle \vec{u}' \cdot \nabla \vec{u}' \rangle \right] = \\ -\nabla \langle p \rangle - \frac{1}{V} \int_{A_f} p dA + \mu_f \left[\nabla^2 \langle \vec{u} \rangle + \frac{1}{V} \int_{A_f} \nabla \vec{u} dA + \nabla \cdot \frac{1}{V} \int_{A_f} \vec{u} dA \right] \end{aligned} \quad (2.26)$$

The last integration on the right hand side of equation (2.26) disappeared due to no stream entrance into solid. Since the pressure term in the momentum equations identified with fluid phase, the Dupuit-Forchheimer relation can be used to change the total volume averaged pressure into the intrinsic volume averaged value.

$$\begin{aligned} \rho_f \frac{\partial \langle \bar{u} \rangle}{\partial t} + \rho_f \left[\frac{1}{\varepsilon} \langle \bar{u} \rangle \cdot \nabla \langle \bar{u} \rangle + \langle \bar{u}' \cdot \nabla \bar{u}' \rangle \right] = \\ -\varepsilon \nabla \langle p \rangle^f - \frac{1}{V} \int_{A_{sf}} p dA + \mu_f \left[\nabla^2 \langle \bar{u} \rangle + \frac{1}{V} \int_{A_{sf}} \nabla \bar{u} dA \right] \end{aligned} \quad (2.27)$$

With rearranging terms and dividing the entire equation to porosity, the macroscopic momentum equation can be written as follows.

$$\begin{aligned} \rho_f \left[\frac{1}{\varepsilon} \frac{\partial \langle \bar{u} \rangle}{\partial t} + \frac{1}{\varepsilon^2} \langle \bar{u} \rangle \cdot \nabla \langle \bar{u} \rangle \right] = -\nabla \langle p \rangle^f + \frac{\mu_f}{\varepsilon} \nabla^2 \langle \bar{u} \rangle \\ - \frac{1}{V} \int_{A_{sf}} p dA + \frac{\mu_f}{\varepsilon} \frac{1}{V} \int_{A_{sf}} \nabla \bar{u} dA - \frac{1}{\varepsilon} \langle \bar{u}' \cdot \nabla \cdot \bar{u}' \rangle \end{aligned} \quad (2.28)$$

The last three terms on the RHS of equation (2.28) can be thought as an additional source terms since they do not exist in the microscopic momentum equations. The last term relates to the effects of inertia while other two terms (3rd and 4th on the RHS) together correspond to viscous effects. Vafai and Tien (Vafai and Tien, 1981) stated that the last three terms in equation (2.28) correspond to Forchheimer-extended Darcy's Law in the following form.

$$\rho_f \left[\frac{1}{\varepsilon} \frac{\partial \langle \bar{u} \rangle}{\partial t} + \frac{1}{\varepsilon^2} \langle \bar{u} \rangle \cdot \nabla \langle \bar{u} \rangle \right] = -\nabla \langle p \rangle^f + \frac{\mu_f}{\varepsilon} \nabla^2 \langle \bar{u} \rangle + S \quad (2.29)$$

$$\bar{S} = -\frac{\mu_f}{K} \langle \bar{u} \rangle - \frac{C}{K^{1/2}} \rho_f \langle \bar{u} \rangle |\langle \bar{u} \rangle| \quad (2.30)$$

Therefore the macroscopic momentum equation gets to be as

$$\begin{aligned} \rho_f \left[\frac{1}{\varepsilon} \frac{\partial \langle \bar{u} \rangle}{\partial t} + \frac{1}{\varepsilon^2} \langle \bar{u} \rangle \cdot \nabla \langle \bar{u} \rangle \right] = \\ -\nabla \langle p \rangle^f + \frac{\mu_f}{\varepsilon} \nabla^2 \langle \bar{u} \rangle - \frac{\mu_f}{K} \langle \bar{u} \rangle - \frac{C}{K^{1/2}} \rho_f \langle \bar{u} \rangle |\langle \bar{u} \rangle| \end{aligned} \quad (2.31)$$

The left hand side (LHS) terms are macroscopic convective inertia terms. The last three terms on the right hand side (RHS) are called as Brinkman (boundary friction),

Darcy (porous viscous) and Forchheimer (porous inertia) terms, respectively (Nakayama, 1995).

2.6. Macroscopic Energy Equations

For a porous medium with two phases as a solid phase and an incompressible Newtonian fluid flowing through the pores without extensive impact of viscous dissipation, the microscopic energy equations for the fluid and solid phases are given in equations (2.4) and (2.5). Volume averaging method can be used to obtain the macroscopic energy equations for the fluid and solid phases of the porous media.

By applying volume averaging method on the microscopic energy equations, following equations for fluid and solid phases can be found as:

$$\rho_f c_{pf} \left(\left\langle \frac{\partial T}{\partial t} \right\rangle + \langle \nabla \cdot \bar{u} T \rangle \right) = k_f \langle \nabla^2 T \rangle \quad (2.32)$$

$$\rho_s c_{ps} \left\langle \frac{\partial T}{\partial t} \right\rangle = k_s \langle \nabla^2 T \rangle \quad (2.33)$$

Utilizing the correspondences given by equations (2.20) and (2.21) on equations (2.32) and (2.33), the macroscopic energy equations can be rewritten as follows.

$$\rho_f c_{pf} \left(\frac{\partial \langle T \rangle}{\partial t} + \nabla \cdot \langle \bar{u} T \rangle + \frac{1}{V} \int_{A_{sf}} \bar{u} T dA \right) = k_f \nabla^2 \langle T \rangle + \nabla \cdot \frac{1}{V} \int_{A_{sf}} k_f T dA + \frac{1}{V} \int_{A_{sf}} k_f \nabla T dA \quad (2.34)$$

$$\rho_s c_{ps} \frac{\partial \langle T \rangle}{\partial t} = k_s \nabla^2 \langle T \rangle + \nabla \cdot \frac{1}{V} \int_{A_{sf}} k_s T dA + \frac{1}{V} \int_{A_{sf}} k_s \nabla T dA \quad (2.35)$$

The integration in the LHS of equation (2.34) vanishes in the light of the non-slip boundary condition at the solid-fluid interface. Since the temperature in both equations demonstrate the temperature of corresponding phases, the representation of intrinsic volume averaged might be better and that's why Dupuit-Forchheimer relation is used

to change equations (2.34) and (2.35). Additionally, equation (2.19) is used to re-compose the second term on the LHS of equation (2.34).

$$\begin{aligned} \rho_f c_{pf} \left(\varepsilon \frac{\partial \langle T \rangle^f}{\partial t} + \nabla \cdot \left[\frac{1}{\varepsilon} \langle T \rangle \langle \bar{u} \rangle \right] + \langle T' \bar{u}' \rangle \right) = \\ k_f \varepsilon \nabla^2 \langle T \rangle^f + \nabla \cdot \left[\frac{1}{V} \int_{A_{sf}} k_f T dA \right] + \frac{1}{V} \int_{A_{sf}} k_f \nabla T dA \end{aligned} \quad (2.36)$$

$$\rho_s c_{ps} (1-\varepsilon) \frac{\partial \langle T \rangle^s}{\partial t} = k_s (1-\varepsilon) \nabla^2 \langle T \rangle^s + \nabla \cdot \left[\frac{1}{V} \int_{A_{sf}} k_s T dA \right] + \frac{1}{V} \int_{A_{sf}} k_s \nabla T dA \quad (2.37)$$

The second term on the LHS of equation (2.36) is rearranged with using macroscopic continuity equation and Dupuit-Forchheimer relation in the following way.

$$\begin{aligned} \nabla \cdot \left[\frac{1}{\varepsilon} \langle T \rangle \langle \bar{u} \rangle + \langle T' \bar{u}' \rangle \right] &= \nabla \cdot \langle T \rangle^f \langle u \rangle + \nabla \cdot \langle T' \bar{u}' \rangle \\ &= \langle u \rangle \cdot \nabla \langle T \rangle^f + \langle T \rangle^f \nabla \cdot \langle u \rangle + \nabla \cdot \langle T' \bar{u}' \rangle = \langle \bar{u} \rangle \cdot \nabla \langle T \rangle^f + \nabla \cdot \langle T' \bar{u}' \rangle \end{aligned} \quad (2.38)$$

With rearranging the terms, the macroscopic equations in terms of intrinsic volume-averaged temperature values can be written as:

$$\begin{aligned} \rho_f c_{pf} \left(\varepsilon \frac{\partial \langle T \rangle^f}{\partial t} + \langle \bar{u} \rangle \cdot \nabla \langle T \rangle^f \right) = \\ k_f \varepsilon \nabla^2 \langle T \rangle^f + \nabla \cdot \left[\frac{1}{V} \int_{A_{sf}} k_f T dA \right] + \frac{1}{V} \int_{A_{sf}} \left[k_f \nabla T dA - \rho_f c_{pf} \nabla \cdot \langle T' \bar{u}' \rangle \right] \end{aligned} \quad (2.39)$$

$$\rho_s c_{ps} (1-\varepsilon) \frac{\partial \langle T \rangle^s}{\partial t} = k_s (1-\varepsilon) \nabla^2 \langle T \rangle^s + \nabla \cdot \left[\frac{1}{V} \int_{A_{sf}} k_s T dA \right] + \frac{1}{V} \int_{A_{sf}} k_s \nabla T dA \quad (2.40)$$

Equation (2.39) and equation (2.40) represents macroscopic form of energy equation for fluid and solid phases respectively. The first terms on the right hand sides of these equations represent the diffusion heat transfer in the fluid and solid phases. The second terms relate to the thermal tortuosity. The last term on the RHS of macroscopic energy

equation of fluid phase (see equation (2.39)) indicates the thermal dispersion showing the additional diffusion heat transfer to the molecular diffusion. The third terms on the RHS of the macroscopic energy equations show the heat transfer between the solid surface and the fluid flowing in the voids and it can be calculated by using the interfacial convective heat transfer concept. Mathematically, the convective heat transfer between solid and fluid can be expressed by using the interfacial heat transfer coefficient.

$$h_{sf} A_{ss} \left(\langle T \rangle^s - \langle T \rangle^f \right) = \frac{1}{V} \int_{A_{sf}} \bar{n} \cdot k_f \nabla T dA = \frac{1}{V} \int_{A_{sf}} \bar{n} \cdot k_s \nabla T dA \quad (2.41)$$

where h_{sf} is the interfacial convective heat transfer coefficient and A_{ss} is the specific solid-fluid interfacial area (i.e., $A_{ss} = A_{sf}/V$). The interfacial convective heat transfer coefficient can be found by using equation (2.42) which directly originates from equation (2.41). At the point that thermal equilibrium breaks down the interfacial convective heat transfer coefficient should be considered for the investigation of macroscopic heat transfer through porous medium.

$$h_{sf} = \frac{\frac{1}{V} \int_{A_{sf}} k_f \nabla T dA}{\langle T \rangle^s - \langle T \rangle^f} \quad (2.42)$$

The important point should be mentioned here is that the interfacial convective heat transfer coefficient is calculated based on the macroscopic temperatures of the solid and fluid phases. Hence it is a macroscopic parameter and it is totally different from the convective heat transfer coefficient usually used in the heat transfer problems with clear fluid flow. By using definition of interfacial convective heat transfer coefficient, equations (2.39) and (2.40) takes the following form:

$$\rho_f c_{pf} \left(\varepsilon \frac{\partial \langle T \rangle^f}{\partial t} + \langle \bar{u} \rangle \cdot \nabla \langle T \rangle^f \right) = \quad (2.43)$$

$$k_f \varepsilon \nabla^2 \langle T \rangle^f + \nabla \cdot \left[\frac{1}{V} \int_{A_{sf}} k_f T dA \right] + h_{sf} A_{ss} \left(\langle T \rangle^s - \langle T \rangle^f \right) - \rho_f c_{pf} \nabla \cdot \langle T' \bar{u}' \rangle$$

$$\rho_s c_{ps} (1 - \varepsilon) \frac{\partial \langle T \rangle^s}{\partial t} = k_s (1 - \varepsilon) \nabla^2 \langle T \rangle^s + \nabla \cdot \left[\frac{1}{V} \int_{A_{sf}} k_s T dA \right] + h_{sf} A_{ss} (\langle T \rangle^s - \langle T \rangle^f) \quad (2.44)$$

In the porous medium, two energy equations which is given above should be solved in order to obtain the macroscopic temperature distribution for each phase if there is local thermal non-equilibrium. There are some circumstances in which Local thermal equilibrium breaks down. The following cases are as an example of this situation.

- Unsteady problems in which heat is transferred from one phase to another,
- when a hot gas flows at a high speed at the entrance region of packed column,
- Applications such that there is considerable difference heat capacities and thermal conductivities between solid and fluid phases
- Applications in which the temperature at the solid-fluid interface changes significantly with respect to time.

CHAPTER 3

CONSIDERED DOMAIN, GOVERNING EQUATIONS AND BOUNDARY CONDITIONS

In this section, the considered porous media for the determination of the impacts of intraparticle porosity on the macroscopic transport parameters are exhibited. The numerical simulation is executed by using governing equations and assigning relevant boundary conditions that the detail explanations is given in this chapter. In the previous chapter the full forms of the governing equations for fluid flow and heat transfer are already introduced. In this part, the equations required to obtain microscopic velocity, pressure and temperature distributions as well as the boundary conditions needed for the solution of the microscopic equations are presented.

3.1. Considered Domain

The geometry of the considered porous media and representative elementary volume (REV) are indicated in Figure 3.1 and Figure 3.2.

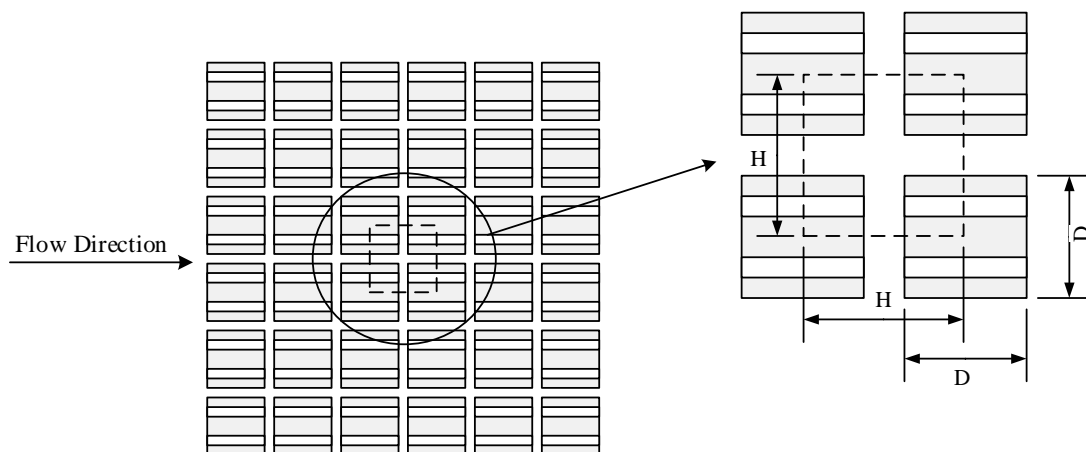
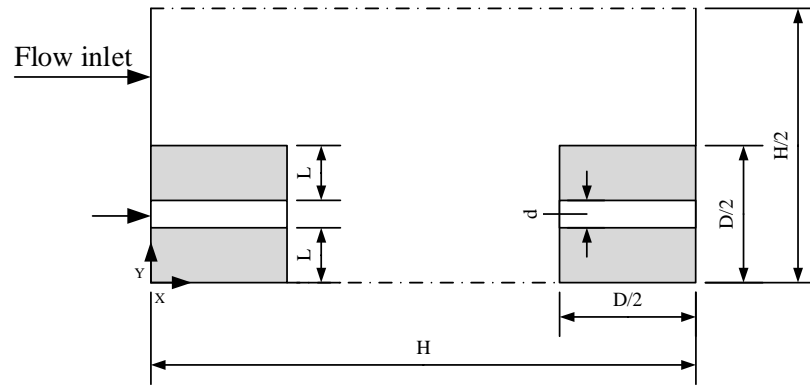
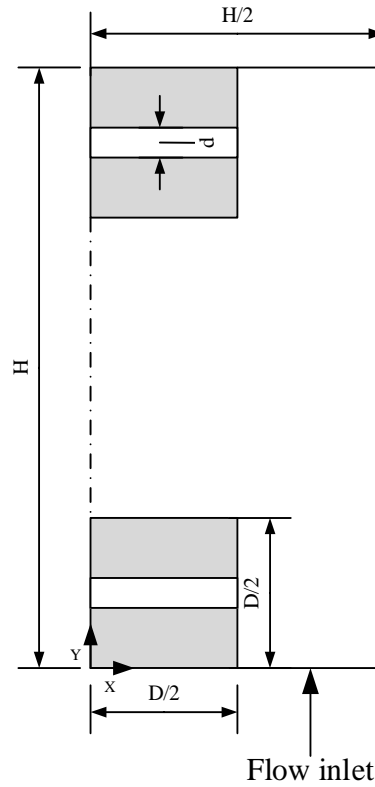


Figure 3.1. The studied dual scale porous medium

A periodical REV with the dimensions of $H \times H$ ($20 \times 20 \text{ mm}^2$) is picked as the computational domain. The geometry is two dimensional in which the square rods are assumed as long in z -direction.



(a)



(b)

Figure 3.2. Computational domains a) half of REV for determination of permeability in x direction b) half of REV for determination of permeability in y direction

The flow in the REV is assumed fully developed and periodical. The permeable square particles are placed with in-line arrangement. There are two symmetrical intraparticle pores considered here which are in longitudinal flow direction for the entire present study. The height of the intraparticle pore is shown by “d” and changes from $0.2D$ to $0.8D$, where D is the size of square particle. The interparticle porosity is changed between 0.4 and 0.75 while the intraparticle porosity varies between 0.2 and 0.8 . The fluid flowing through the medium is assumed to be Newtonian and incompressible with

constant thermophysical properties. The flow is laminar and in Darcian region ($Re \leq 1$). The study is performed for air with density of 1.225 kg/m^3 and viscosity of $17.894 \cdot 10^{-6} \text{ kg/ms}$.

Some example of REV displaying the change of intraparticle porosity for the constant value of interparticle porosity are shown in Figure 3.3.

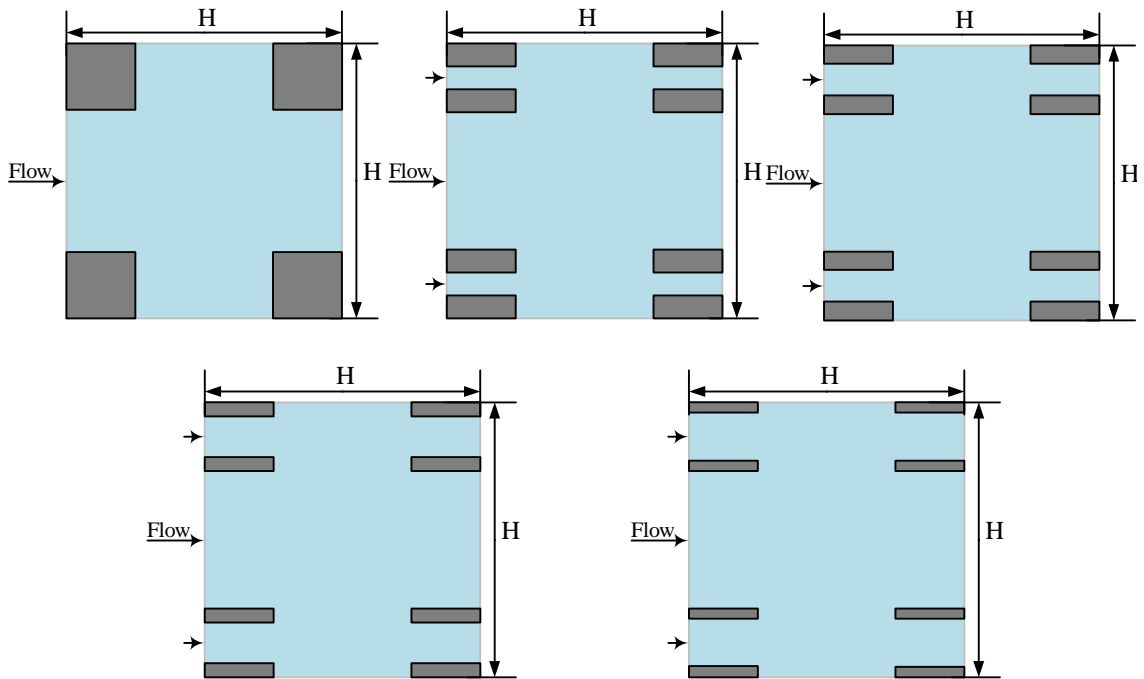


Figure 3.3. REV with different intraparticle size of 0, 0.2, 0.4, 0.6 and 0.8 for $\varepsilon_f = 0.75$

3.2. Governing Equations and Boundary Conditions for Determination of Permeability

Bu analyzing microscopic governing equations, permeability of fluid passing through the REV is determined. The fluid flow in inter- and intraparticle pores is assumed incompressible and steady. The continuity and momentum equations are solved in order to determine the velocity and pressure distributions in the pores. These equations in Cartesian coordinate can be written as:

$$\frac{\partial u}{\partial x} + \frac{\partial v}{\partial y} = 0 \quad (3.1)$$

$$u \frac{\partial u}{\partial x} + v \frac{\partial u}{\partial y} = -\frac{1}{\rho} \frac{\partial p}{\partial x} + \nu \left(\frac{\partial^2 u}{\partial x^2} + \frac{\partial^2 u}{\partial y^2} \right) \quad (3.2)$$

$$u \frac{\partial v}{\partial x} + v \frac{\partial v}{\partial y} = -\frac{1}{\rho} \frac{\partial p}{\partial y} + \nu \left(\frac{\partial^2 v}{\partial x^2} + \frac{\partial^2 v}{\partial y^2} \right) \quad (3.3)$$

where u and v are the velocity components in x and y directions and p is the pressure, ρ and ν are density and kinematic viscosity of fluid, respectively.

In order to solve equations (3.1), (3.2) and (3.3) knowing the boundary conditions for velocities at the boundaries of REV and at the fluid-solid interfaces are necessary

3.2.1. Determination of Intrinsic Intraparticle Permeability

The intrinsic intraparticle permeability is valid only for x direction and calculated for a single permeable particle without considering the effect of interparticle flow. The intraparticle permeability is calculated based on velocity field obtained from continuity and momentum equations with the following boundary conditions:

$$\text{On solid walls:} \quad u = v = 0 \quad (3.4)$$

$$\text{For inlet an outlet boundaries:} \quad u(0, y) = f(y), \quad \frac{\partial u(0, y)}{\partial x} = \frac{\partial v(D/2, y)}{\partial x} = 0 \quad (3.5)$$

As it is well known, the permeability depends on the micro-structure of the solid phase in the porous media and it is independent of the properties of the fluid. Permeability is a tensor quantity and for a two dimensional flow in Cartesian coordinate and it can be defined as:

$$\begin{pmatrix} \langle u \rangle \\ \langle v \rangle \end{pmatrix} = \frac{1}{\mu} \begin{pmatrix} K_{xx} & K_{yx} \\ K_{xy} & K_{yy} \end{pmatrix} \begin{pmatrix} \frac{\partial p}{\partial x} \\ \frac{\partial p}{\partial y} \end{pmatrix} \quad (3.6)$$

where $K_{xy}, K_{yx}, K_{xy}, K_{xy}$ are components of the permeability.

The Darcy velocity and pressure gradient for flow through the quarter of intraparticle pore is calculated by following relations:

$$\langle u_p \rangle = \frac{4}{D^2} \int_L^{L+d} \int_0^{D/2} u \, dx \, dy \quad (3.7)$$

$$-\frac{d\langle p \rangle^f}{dx} = \frac{2}{Dd} \left[\int_L^{L+d} p|_{x=0} \, dy - \int_L^{L+d} p|_{x=D/2} \, dy \right] \quad (3.8)$$

For the intrinsic intraparticle permeability the permeability tensor takes the following form:

$$\begin{pmatrix} \langle u_p \rangle \\ \langle v_p \rangle \end{pmatrix} = \frac{1}{\mu} \begin{pmatrix} K_{p,xx} & 0 \\ 0 & 0 \end{pmatrix} \begin{pmatrix} \frac{\partial p}{\partial x} \\ \frac{\partial p}{\partial y} \end{pmatrix} \quad (3.9)$$

where $K_{p,xx}$ is the permeability component in longitudinal direction. The value of $K_{p,xy}$ and $K_{p,yx}$ are equal, and the value of $K_{p,yy}$ component is vanished since there is no flow in transverse direction (vertical direction).

3.2.2. Determination of Intrinsic Interparticle Permeability

The intrinsic interparticle permeability (without considering of the intraparticle pores) is found by using the continuity and momentum equations with following boundary conditions for flow in x direction:

On solid walls: $u = v = 0$ (3.10)

For inlet and outlet boundaries: $u(0, y) = f(y), v(0, y) = 0$ and $\frac{\partial u(H, y)}{\partial x} = \frac{\partial v(H, y)}{\partial x} = 0$ (3.11)

The Darcy velocity and pressure gradient in x direction for flow through the half of REV is calculated by following relation:

$$\langle u_f \rangle = \frac{2}{H^2} \int_0^{H/2} \int_0^H u \, dx \, dy \quad (3.12)$$

$$-\frac{d\langle p \rangle^f}{dx} = \frac{2}{H(H-D)} \left[\int_{D/2}^{(H-D)/2} p|_{x=0} \, dy - \int_{D/2}^{(H-D)/2} p|_{x=H} \, dy \right] \quad (3.13)$$

For the intrinsic interparticle permeability, the permeability tensor takes the following form:

$$\begin{pmatrix} \langle u_f \rangle \\ \langle v_f \rangle \end{pmatrix} = \frac{1}{\mu} \begin{pmatrix} K_{f,xx} & 0 \\ 0 & K_{f,yy} \end{pmatrix} \begin{pmatrix} \frac{\partial p}{\partial x} \\ \frac{\partial p}{\partial y} \end{pmatrix} \quad (3.14)$$

For the studied case the values of $K_{f,xx}$ and $K_{f,yy}$ are equal to each other due to symmetrical geometry of REV.

3.2.3. Determination of Bulk Permeability

The bulk permeability in x and y directions are different, that's why they should be calculated for both sides. The bulk permeability is determined by solution of the governing equations and boundary conditions.

For the determination of the permeability in the horizontal direction:

On solid walls: $u = v = 0$ (3.15)

For top and bottom boundaries: $\frac{\partial u}{\partial y} = \frac{\partial v}{\partial y} = 0$ (3.16)

For inlet and outlet boundaries: $u(0, y) = f(y), v(0, y) = 0$ and $\frac{\partial u(H, y)}{\partial x} = \frac{\partial v(H, y)}{\partial x} = 0$ (3.17)

For determination of the permeability in the vertical direction:

$$\text{On solid walls:} \quad u = v = 0 \quad (3.18)$$

$$\text{For left and right boundaries:} \quad \frac{\partial u}{\partial x} = \frac{\partial v}{\partial x} = 0 \quad (3.19)$$

$$\text{For inlet and outlet boundaries:} \quad v(x, 0) = f(x), u(x, 0) = 0 \text{ and } \frac{\partial u(x, H)}{\partial y} = \frac{\partial v(x, H)}{\partial y} = 0 \quad (3.20)$$

The functions of $f(x)$ and $f(y)$ is the velocity profile for the inlet boundary of the REV. After obtaining periodic velocity field in the structural units, the macroscopic velocities (Darcian velocities) are calculated by using following equations:

$$\langle u_b \rangle = \frac{2}{H^2} \int_0^{H/2} \int_0^H u \, dx \, dy \quad (3.21)$$

$$\langle v_b \rangle = \frac{2}{H^2} \int_0^{H/2} \int_0^H v \, dy \, dx \quad (3.22)$$

For determination of permeability in x and y direction, the pressure drop throughout the REV is found by following relations:

$$-\frac{d\langle p \rangle^f}{dx} = \frac{1}{H} \left[\frac{\int_L^{L+d} p|_{x=0} \, dy + \int_{D/2}^{H/2} p|_{x=0} \, dy}{(H-D)/2+d} - \frac{\int_L^{L+d} p|_{x=H} \, dy + \int_{D/2}^{H/2} p|_{x=H} \, dy}{(H-D)/2+d} \right] \quad (3.23)$$

$$-\frac{d\langle p \rangle^f}{dy} = \frac{2}{H(H-D)} \left[\int_{D/2}^{(H-D)/2} p|_{y=0} \, dx - \int_{D/2}^{(H-D)/2} p|_{y=H} \, dx \right] \quad (3.24)$$

The first term of the right hand side of equation (3.24) is the integral of pressure in inlet while the second term gives the integral of pressure drop in the outlet of REV. Permeability is a tensor quantity and for bulk permeability it can be given as follows:

$$\begin{pmatrix} \langle u_b \rangle \\ \langle v_b \rangle \end{pmatrix} = \frac{1}{\mu} \begin{pmatrix} K_{b,xx} & 0 \\ 0 & K_{b,yy} \end{pmatrix} \begin{pmatrix} \frac{\partial p}{\partial x} \\ \frac{\partial p}{\partial y} \end{pmatrix} \quad (3.25)$$

Since the structure of REV in x and y directions are different, hence $K_{xx} \neq K_{yy}$.

3.3. Governing Equations and Boundary Conditions for Determination of Interfacial Convective Heat Transfer Coefficient

Microscopic form of energy equation of fluid is utilized besides of the motion equations for the determination of the interfacial convective heat transfer coefficient. The governing equations are solved under the assumptions of local thermal non-equilibrium between solid and fluid phases, a uniform and constant temperature distribution in the solid phase and steady state condition. The calculations are done for $10 \leq Re \leq 600$. Moreover, the energy equation for the solid phase is not considered.

$$\rho_f c_{pf} \left(u \frac{\partial T}{\partial x} + v \frac{\partial T}{\partial y} \right) = k_f \left(\frac{\partial^2 T}{\partial x^2} + \frac{\partial^2 T}{\partial y^2} \right) \quad (3.26)$$

For the solution of equation (3.26), temperature boundary conditions at the boundaries of REVs and at the interfaces of solid and fluid phases are required. As can be seen from Figure 3.2 (a), the boundary conditions for the microscopic energy equation for fluid phase are chosen as symmetry for the top and the bottom of the REV. The temperature gradient at the fluid outlet boundary is zero, therefore no diffusion transport exists. Finally, periodic temperature profiles are generated for the inlet and outlet boundaries. The employed boundary conditions in a mathematical statement can be written as follows:

$$\text{In the solid phase:} \quad T_s = \text{Constant} \quad (3.27)$$

$$\text{On the fluid-solid interfaces:} \quad T = T_s \quad (3.28)$$

For the top and the bottom boundaries:
$$\frac{\partial T}{\partial y} = 0 \quad (3.29)$$

For the inlet boundary:
$$T = g(y) \quad (3.30)$$

For the outlet boundary:
$$\frac{\partial T}{\partial x} = 0 \quad (3.31)$$

The temperature profile and thermal periodicity of the REV is given by $g(y)$ function. The microscopic temperature distribution in the fluid phase is obtained by applying the boundary conditions and solving the microscopic energy equation for the REV with periodic boundaries. At that point, to compute the value of the interfacial convective heat transfer coefficient equation (2.42) can be used.

The equation (2.42) indicates that, macroscopic temperatures of both phases are compulsory to figure the interfacial convective heat transfer coefficient. There is equality between macroscopic temperature of the solid phase and selected reference temperature value. However, the macroscopic temperature of the fluid phase can be ascertained by utilizing intrinsic volume averaging on the microscopic temperature.

$$\langle T \rangle^s = T_{ref} \quad (3.32)$$

$$\langle T \rangle^f = \frac{1}{V_f} \int_{V_f} T dV \quad (3.33)$$

The interfacial Nusselt number can be defined as follows:

$$Nu = \frac{h_{sf} H}{k_f} \quad (3.34)$$

As can be seen from equation (3.34) in this study the dimension of the REV is selected as characteristic length to define Nusselt number. The same manner is also observed in numerous reported studies. ((Ozgumus and Mobedi, 2014), (Nakayama et al., 2002), (Alshare et al., 2010), (Lopez Penha et al., 2012)).

CHAPTER 4

SOLUTION TECHNIQUE AND COMPUTATIONAL DETAILS

In this chapter, the numerical solution technique used to solve the governing equations is explained in detail. The details of iterative procedures employed to obtain the hydraulically and thermally periodical boundary conditions, computational method and employed parameters for the considered REV are introduced in this chapter. The performed grid independency validation for the numerical computation of the macroscopic transport parameters is also checked.

4.1. Numerical Procedure

In this section the iterative procedures used to reach periodical heat and fluid flow are explained in details. Different iterative procedures are applied to determine hydraulically and thermally fully developed flow. The corresponding velocity, pressure and temperature distributions are obtained and illustrate in the following parts.

4.1.1. Iterative Procedure for Obtaining Periodical Fluid Flow Boundaries

In Section 3.2 the periodical boundary conditions which can be found by using an iterative procedure was given. As mentioned before, the function $f(y)$ provides hydraulic periodicity for the inlet and outlet boundaries of the considered REV. This iterative procedure is displayed in Figure 4.1 and explained in the following way.

The Figure 4.1 shows the inlet and outlet velocity profiles obtained for determination of the bulk permeability. Firstly, a uniform velocity profile is assumed as seen from Figure 4.1. After solving the governing equations and obtaining the velocity field, the outlet velocity profile of first run is used as the inlet boundary condition for second run and the problem is solved again. This iteration continues until the same

velocity profiles at the inlet and outlet boundaries achieved. By this way, the periodicity of the velocity field is attained. The same method is applied for obtaining flow periodicity in y direction.

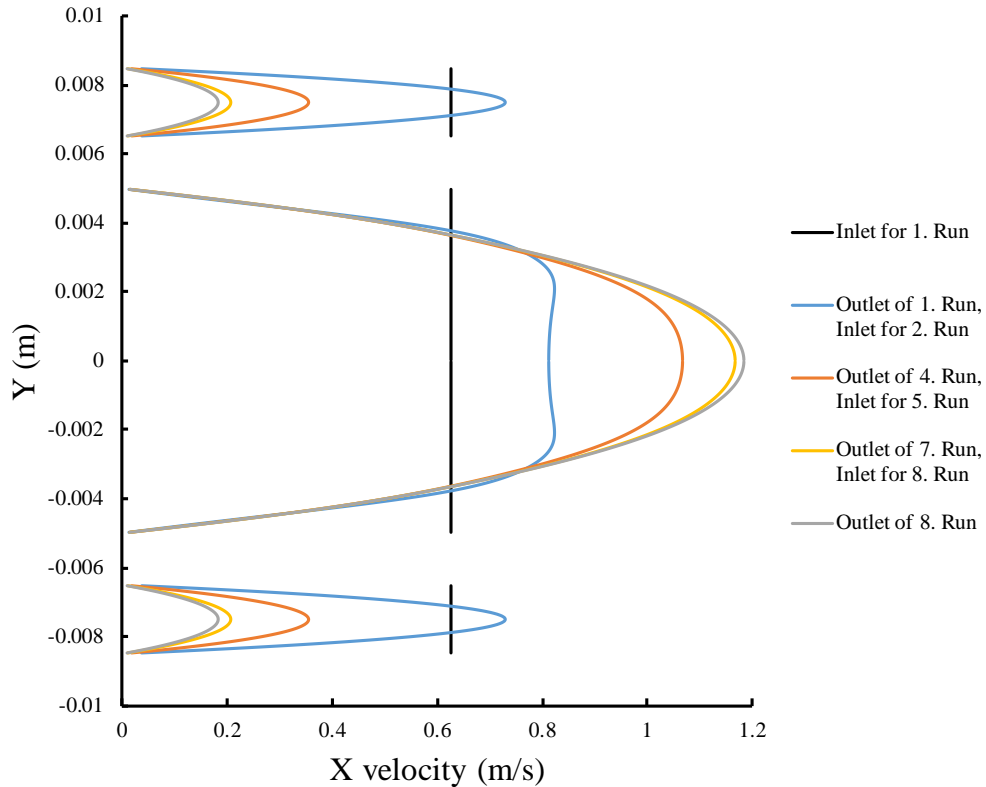


Figure 4.1. The change of velocity profile to obtain fully developed condition

Moreover, the periodicity of the flow boundaries is assumed to be valid when the relative difference between the results of the permeability values obtained in the successive iterations become negligible.

4.1.2. Iterative Procedure for Obtaining Periodical Thermal Boundaries for Determination of Interfacial Convective Heat Transfer Coefficient

To compute the interfacial convective heat transfer coefficient, periodical temperature boundaries should be subsist at the inlet and outlet boundaries of the REV because of infinite periodical structure of porous medium. Therefore, the boundary conditions given in Section 3.3 are the periodical boundary conditions and the temperature profile function $g(y)$, which is established at the inlet fluid boundary

provides thermal periodicity of the inlet and outlet boundaries of the REV. This function is found by the accompanying technique;

- Toward the start of this iterative procedure, a uniform temperature, different from the solid temperature is defined for the fluid inlet boundary (as can be seen from Figure 4.2)
- The temperature field for the whole fluid space is acquired by solving the energy equation for fluid.
- The temperature profile for the inlet of the next computation is determined from the dimensionless temperature profile at the outlet boundary of the last iteration.
- The iterative process will be terminated when dimensionless temperature distribution between the inlet and outlet and no variety of the interfacial Nusselt number are seen. Since a thermally fully- developed convection heat transfer is valid, no change of the dimensionless temperature and interfacial convective heat transfer should be observed in the sequential REV's through the flow direction in the porous medium.

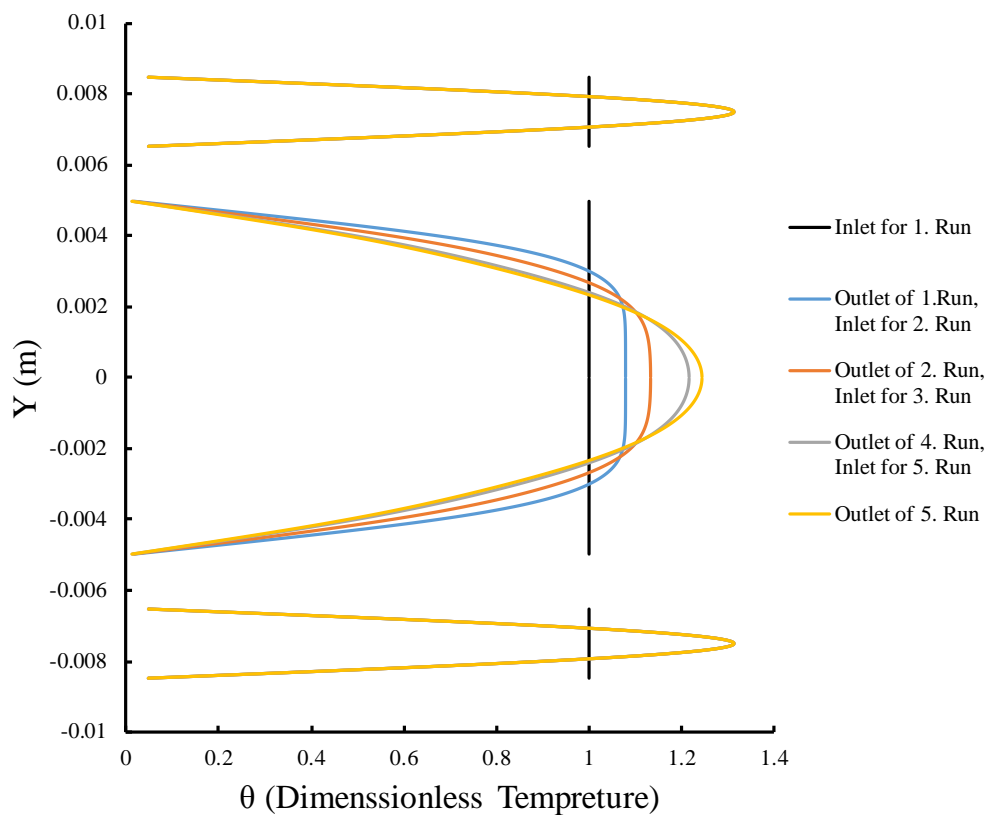


Figure 4.2. The change of temperature profile to obtain thermally fully developed condition

The dimensionless temperature is defined by equation (4.1).

$$\theta(y) = \frac{T(y) - T_s}{T_b - T_s} \quad (4.1)$$

where T_s and T_b are the solid and bulk temperatures, respectively. T_b is defined as follows:

$$T_b = \frac{\int uTdy}{\int udy} \quad (4.2)$$

4.2. Computational Details

The pore level flow equations are solved for the studied REV's. The number of grids is chosen as 400x400 for the entire domain. A commercial code based on finite volume method is used to solve the governing equations, computationally (ANSYS/Fluent 15). The power law scheme is employed to treat the discretization of the convection terms in the momentum and energy equation SIMPLE method is used for handling the pressure-velocity coupling. The approximate errors (Residuals) are set to 10^{-9} for flow variables and 10^{-12} for temperature.

4.3. Grid Independency Tests

Grid independency study is done to select the best grid size for the exact computation of permeability and interfacial convective heat transfer coefficient. The change of dimensionless permeability with grid size is shown in Figure 4.3 for cases with $\varepsilon_f = 0.75$ ($\varepsilon_p = 0.2$) and $\varepsilon_f = 0.4$ ($\varepsilon_p = 0.8$) when $Re = 0.01$. As can be seen from the figure, discretization with grid number of 160000 is sufficient to achieve acceptable results. In fact, for low Reynolds number flows, lower grid sizes are proper for capturing the accurate dimensionless permeability values. However, the computations of the interfacial convective heat transfer coefficients are made for high Reynolds numbers in addition to the lower ones. Consequently, 400x400 grid size is decided for using in all computations.

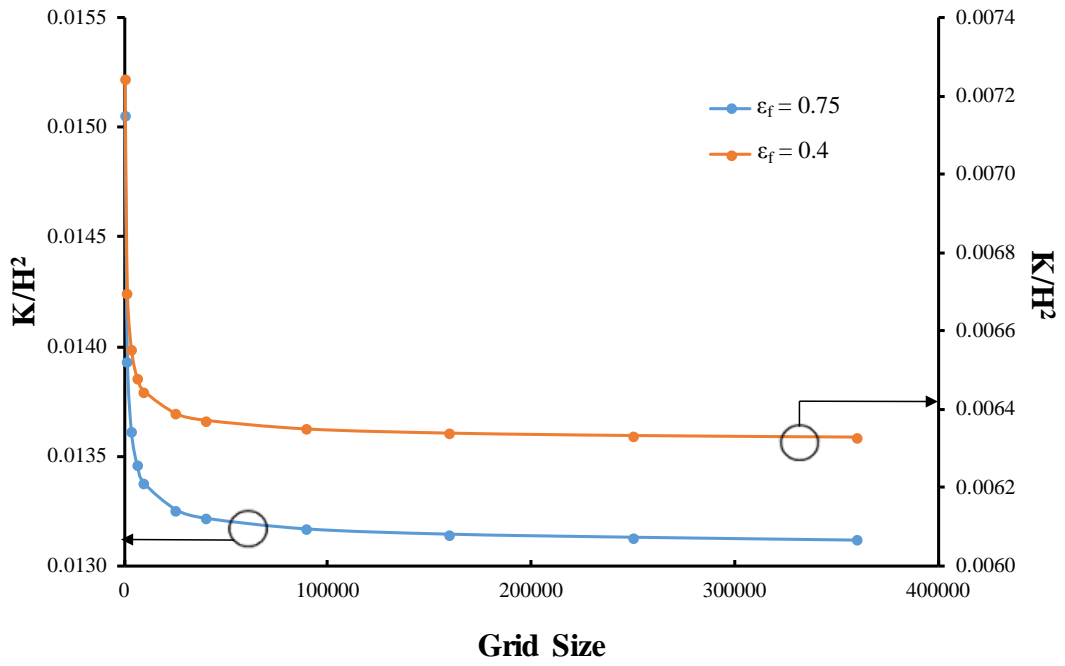


Figure 4.3. The change of dimensionless permeability with grid number for two dual scale porous media; $\epsilon_f = 0.75$, $\epsilon_p = 0.2$ and $\epsilon_f = 0.4$, $\epsilon_p = 0.8$

CHAPTER 5

RESULTS AND DISCUSSION

In this chapter the results for permeability, Kozeny constant, interfacial convective heat transfer have been presented and discussed. Firstly, the validation of numerical model out comes is compared with the results of reported studies in the literature. Afterwards, results of the fluid flow and heat transfer computations are presented in the next sections individually.

5.1. Validation of Results

Before starting to investigate the effects of intraparticle porosity on the permeability and interfacial convective heat transfer coefficient, some porous structures reported in the literature are selected. Hence to approve the validations of numerical computations, the obtained results are compared with the results of the reported studies.

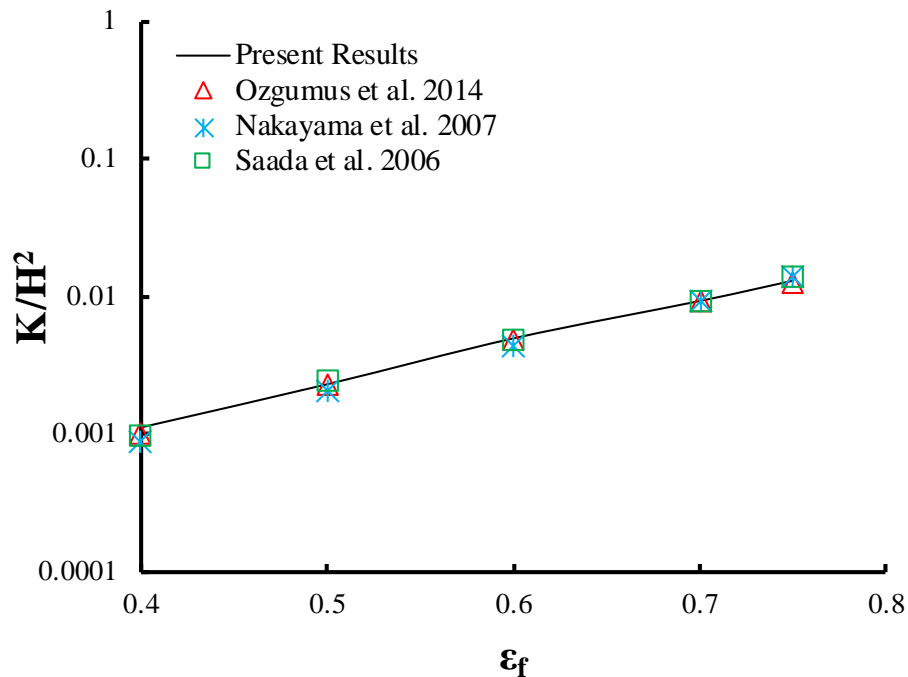


Figure 5.1. Comparison of dimensionless permeability obtained in this study with the results reported in literature

In Figure 5.1 the obtained dimensionless permeability for porous media with impermeable particle are compared with the values reported by Ozgumus et al. (Ozgumus et al., 2014), Saada et al. (Saada et al., 2005) and (Nakayama et al., 2007) for square rod porous media when $\phi = 0.75$. As seen from the figure, the obtained values of the present study and the reported literature values are in good agreement.

In the wake of accepting the numerical results of motion equations, the validation is also performed for the computation of the interfacial convective heat transfer coefficient by solving the microscopic energy equation of fluid phase and the Navier-Stokes equations. For the examination, the porous media with square rods in inline arrangement and porosity of 0.75 is created. After solving the equations the interfacial Nusselt numbers found for this porous media are compared with the results of Ozgumus and Mobedi (Ozgumus and Mobedi, 2014), Nakayama et al. (Nakayama et al., 2002), Lopez Penha et al. (Lopez Penha et al., 2012) and Gamrat et al. (Gamrat et al., 2008) and the comparison is shown in Figure 5.2. As can be detected from Figure 5.2, there is similarity between the results of present study and the literature results for an extensive variety of Reynolds number.

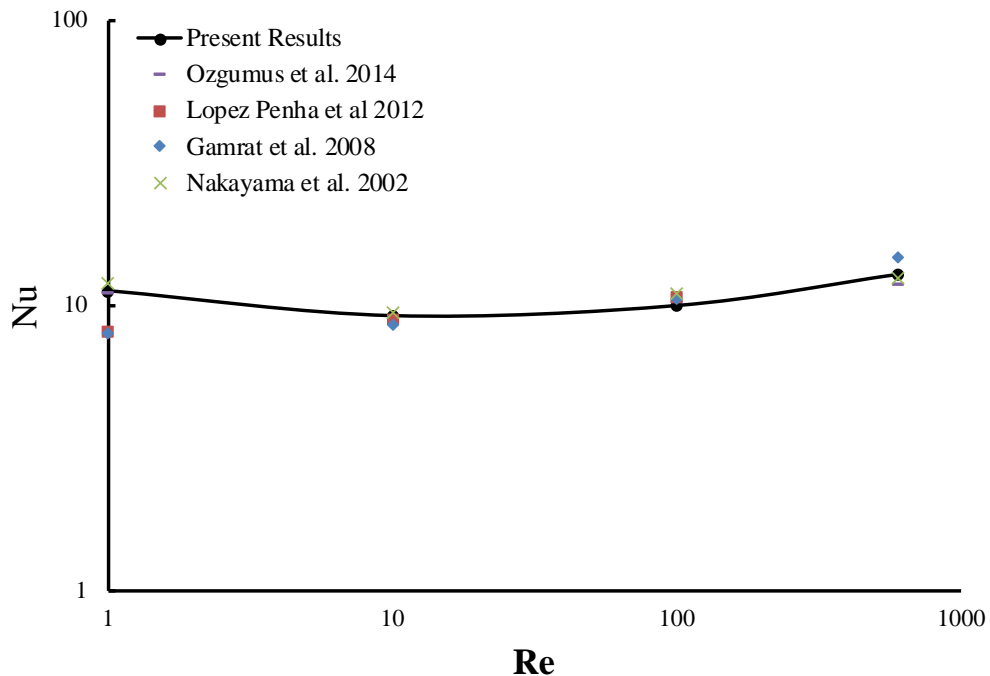


Figure 5.2. Comparison of the obtained results for the change of interfacial Nusselt number with the results of the reported studies

5.2. Results for Permeability and Kozeny Constant

Figure 5.3 shows the change of dimensionless pressure drop with different Reynolds number ($0.01 < Re < 1$) for two porous media as $\varepsilon_f = 0.75, \varepsilon_p = 0.2$ and $\varepsilon_f = 0.4, \varepsilon_p = 0.8$. As well known, for small values of Reynolds number, the permeability does not change with flow and it should remain constant. This figure shows that Darcy equation is valid and inertia effect is negligible for all results obtained in this study.

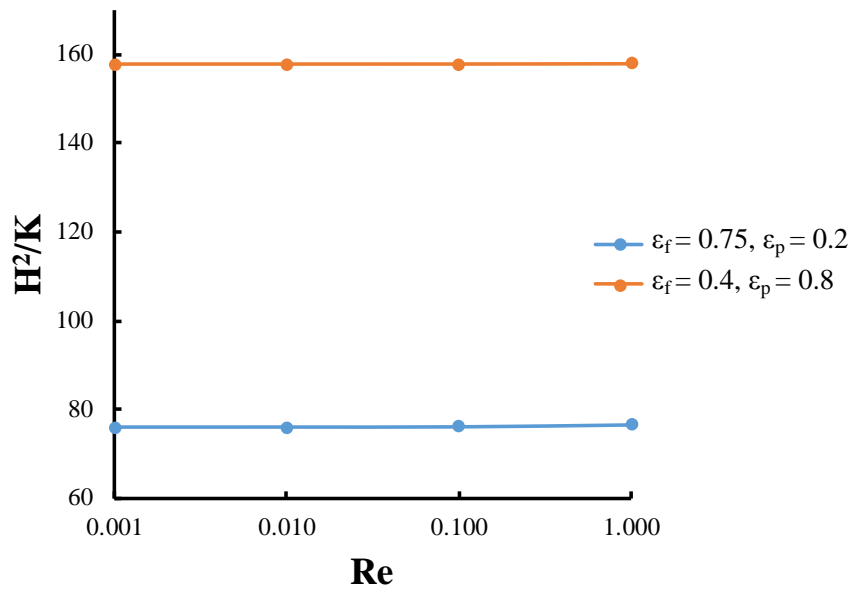


Figure 5.3. Change of permeability with Reynolds number for two dual scale porous media; $\varepsilon_f = 0.75, \varepsilon_p = 0.2$ and $\varepsilon_f = 0.4, \varepsilon_p = 0.8$

The intrinsic and bulk permeabilities both in x and y directions are found and presented in the following section, separately.

5.2.1. Permeability in x Direction

Figure 5.4 shows the streamlines and normalized pressure distributions in inter and intraparticle pores of dual scale porous media with different intraparticle porosities when $\varepsilon_f = 0.75$. In this figure, the pressure of each porous media is added with a constant value such that the inlet pressure values of all REV's become identical. Then, the normalization is done by dividing of the pressure in entire REV with the identical inlet

pressure value. Figure 5.4 (a) shows the streamlines and pressure distribution for a dual scale porous medium with $\varepsilon_p = 0.2$. As seen, inter and intraparticle flows provide the fluid transfer from one REV to another as a result of pressure gradient. The secondary flows occur in the top and bottom gaps between two rods. Figure 5.4 (b) shows the flow patterns in the REV of the same porous media however the intraparticle porosity is increased to 0.4. The same types of flows are also observed for this porous structure. The flow rate in intraparticle region increases, however, the size of the secondary flows in the top and bottom gaps decreases. In Figure 5.4 (c) and (d), the intraparticle porosity increases to $\varepsilon_p = 0.6$ and 0.8, respectively and the interparticle porosity remains constant. The secondary flows on the top and bottom of the REV's disappear and the flow rate of intraparticle becomes comparable with the rate of interparticle flow.

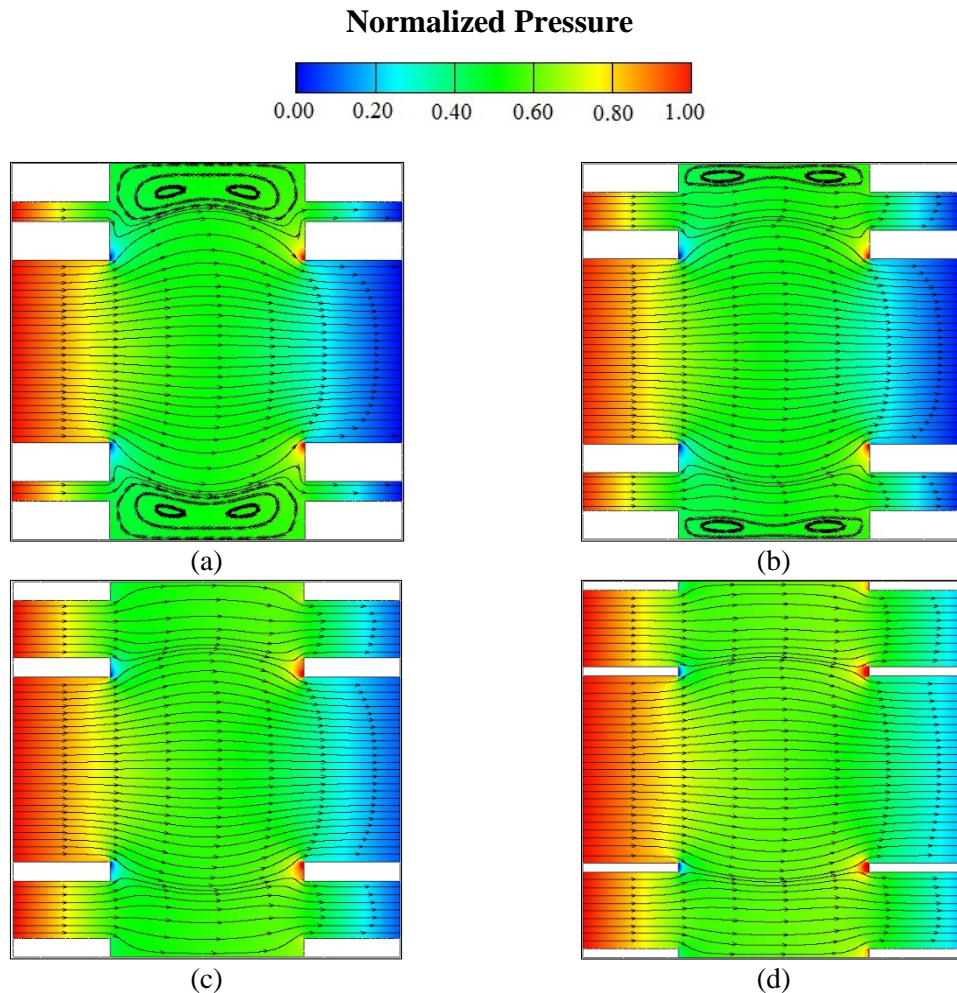


Figure 5.4. The streamlines and pressure contours for flow in x direction in dual scale porous media with $\varepsilon_f = 0.75$ a) $\varepsilon_p = 0.2$, b) $\varepsilon_p = 0.4$, c) $\varepsilon_p = 0.6$, d) $\varepsilon_p = 0.8$

In Figure 5.5, the streamlines and pressure distributions in the interparticle and intraparticle pores of dual scale porous media with different intraparticle porosities when $\varepsilon_f = 0.4$ are shown. Figure 5.5 (a) shows the streamlines and pressure distribution for a dual scale porous medium with $\varepsilon_p = 0.2$. The interparticle flow is dominant in the horizontal direction. The secondary flows occur in the top and bottom gaps are compressed by the intraparticle flows. The main flow passes through the interparticle region while the rate of flow in the intraparticle pores are smaller. Figure 5.5 (b) indicates the flow patterns in REV with $\varepsilon_p = 0.4$ for the same interparticle porosity. The size of the secondary flow decreases and flow rate passes through the intraparticle region increases. Figure 5.5 (c) and (d) are plotted for extreme cases for which the intraparticle porosities are 0.6 and 0.8. It is observed that the fluid flows through inter and intraparticle parts are comparable or even the intraparticle flow rate is greater than interparticle one.

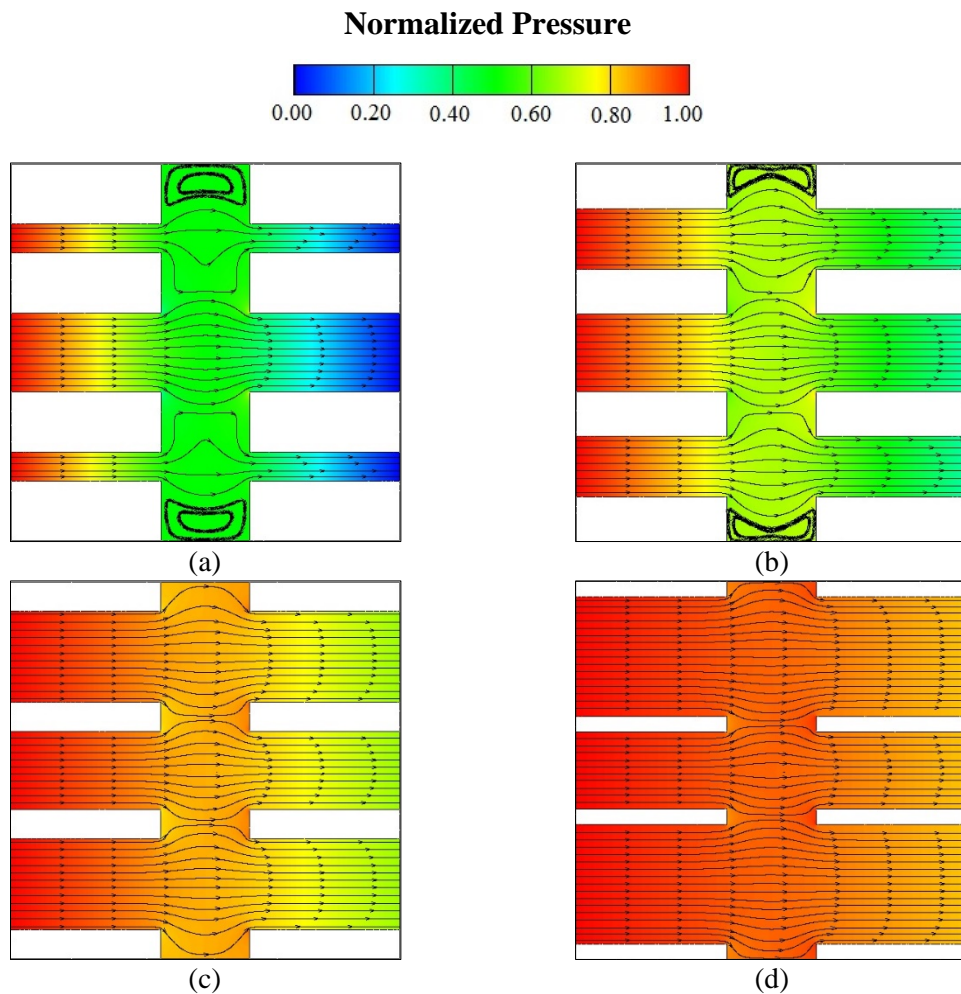


Figure 5.5. The streamlines and pressure contours for flow in x direction in dual scale porous media with $\varepsilon_f = 0.4$ a) $\varepsilon_p = 0.2$, b) $\varepsilon_p = 0.4$, c) $\varepsilon_p = 0.6$, d) $\varepsilon_p = 0.8$

The variations of intrinsic interparticle, intraparticle and bulk permeabilities with intraparticle porosity are illustrated in Figure 5.6. In Figure 5.6 (a), the change of permeability values for $\varepsilon_f = 0.75$ is shown. As seen, the value of intrinsic interparticle permeability is constant while the value of intrinsic intraparticle permeability increases with the increase of ε_p . The values of interparticle and bulk permeabilities are higher than the intraparticle permeability even for $\varepsilon_p = 0.8$. When the ε_f becomes 0.6 (Figure 5.6 (b)), the value of intrinsic interparticle permeability becomes lower than the ones of $\varepsilon_f = 0.75$. The values of intrinsic intraparticle and interparticle permeabilities become closer to each other for $\varepsilon_p = 0.8$. The change of permeability with ε_p for the interparticle porosity of 0.5 is revealed in Figure 5.6 (c). The same trend of increasing K_p with ε_p observed in Figure 5.6 (a) and (b), can also be seen. However, for $\varepsilon_p = 0.5$, the intrinsic inter- and intraparticle permeabilities become equal at a point around $\varepsilon_p = 0.6$. After this value of ε_p , the value of K_p increases and it becomes greater than interparticle permeability. For $\varepsilon_p = 0.8$, the values of K_p and bulk permeability becomes closer to each other. Figure 5.6 (d) indicates the permeability variations with ε_p for interparticle porosity of 0.4. For the intraparticle porosity greater than 0.4, the effect of intrinsic intraparticle permeability is greater than K_f since the fluid flows mainly through intraparticle pores. The domination of intraparticle respect to interparticle permeability for $\varepsilon_f = 0.4$ and $\varepsilon_p = 0.8$ can be observed from streamlines in Figure 5.5 (d).

Figure 5.7 shows the change of $K_{b,xx} / K_{f,xx}$ with intraparticle porosity for different values of interparticle porosity. As can be seen, for high values of interparticle porosity the effect of intra pores is negligible and the value of bulk permeability remains almost constant. Hence, creating intraparticle channels or pores does not influence the bulk permeability. For a porous media with $\varepsilon_f = 0.75$, creating intraparticle pore with $\varepsilon_p = 0.8$ can increase the bulk permeability only 23%. For the low values of interparticle porosity the effect of intraparticle pores becomes visible. For a porous media with $\varepsilon_f = 0.4$, creating pores with the porosity of $\varepsilon_p = 0.4$ can increase the bulk permeability with 464%.

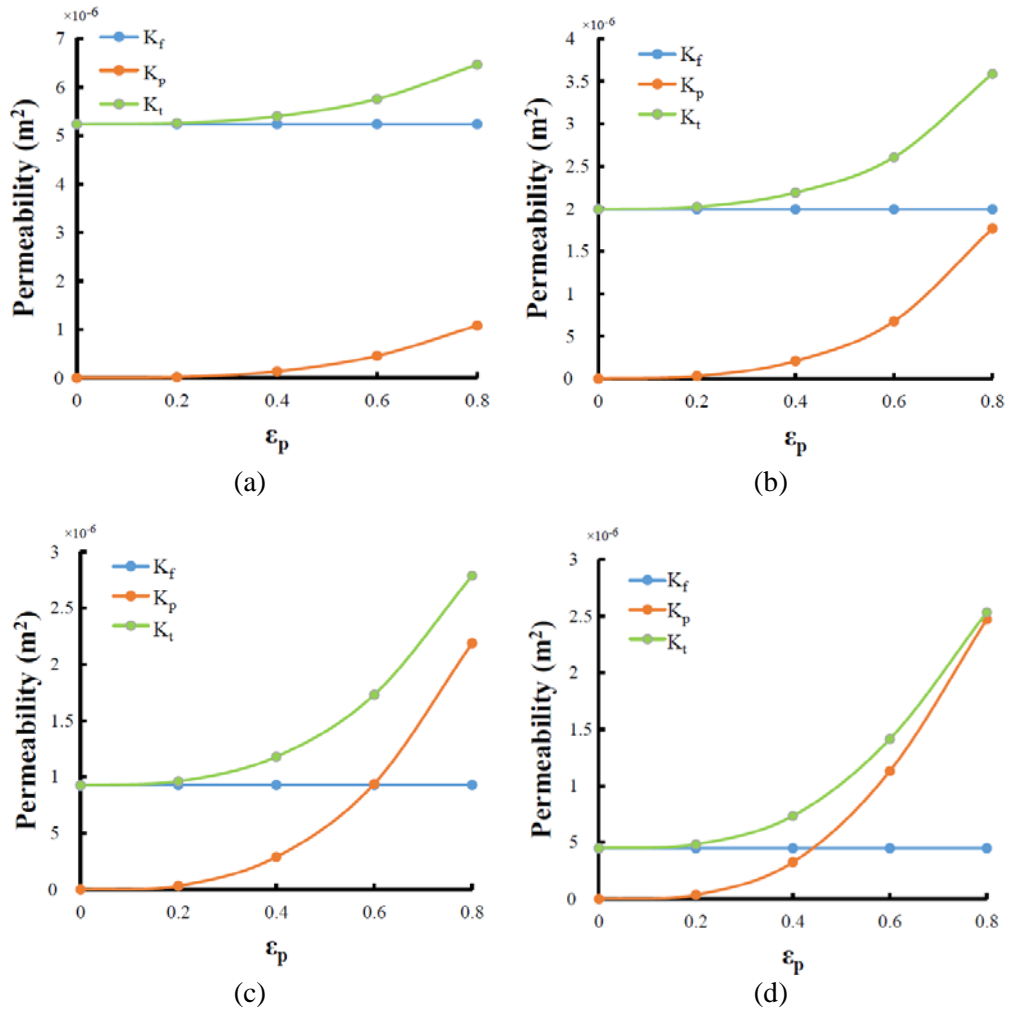


Figure 5.6. The change of intrinsic interparticle, intraparticle and bulk permeabilities with intraparticle porosity a) $\epsilon_f = 0.75$, b) $\epsilon_f = 0.6$, c) $\epsilon_f = 0.5$, d) $\epsilon_f = 0.4$

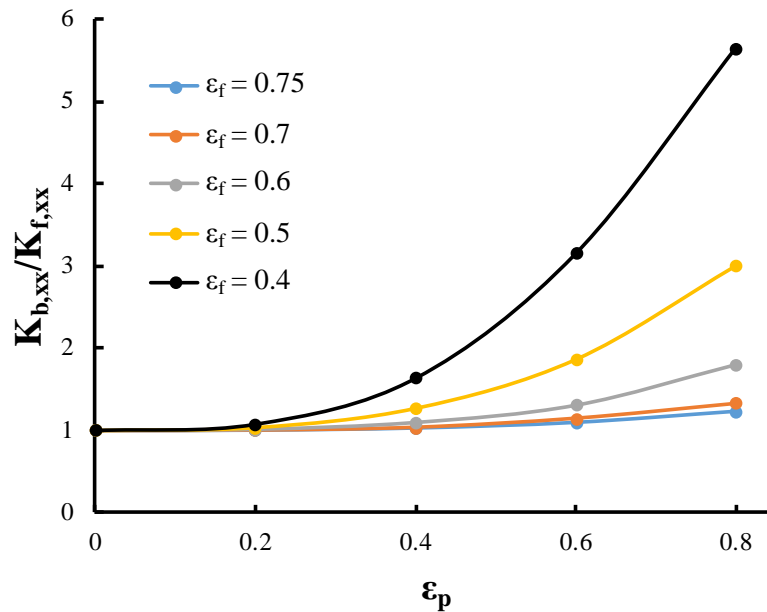


Figure 5.7. Change of $K_{b,xx} / K_{f,xx}$ with intraparticle porosity for different values of interparticle porosity

In Figure 5.8, the variation of $K_{b,xx} / D^2$ with $\varepsilon_f^3 / (1 - \varepsilon_f)^2$ for different intraparticle porosities is shown. For mono scale porous medium ($\varepsilon_p = 0$) the change of $K_{b,xx} / D^2$ with $\varepsilon_f^3 / (1 - \varepsilon_f)^2$ seems linear as expected from Kozeny-Carman equation. As the intraparticle porosity increases, the linear relationship between $K_{b,xx} / D^2$ and $\varepsilon_f^3 / (1 - \varepsilon_f)^2$ disappears. As seen, the value of $K_{b,xx}$ increases with ε_f , however the rate of increase is different and it is function of ε_p . For the large values of $\varepsilon_f^3 / (1 - \varepsilon_f)^2$, the change of bulk permeability with intraparticle porosity is very small since the size of particles is small in the REV. For small values of $\varepsilon_f^3 / (1 - \varepsilon_f)^2$, the effect of ε_p is considerable since the size of particles and consequently the volume of intraparticle pores in REV become larger.

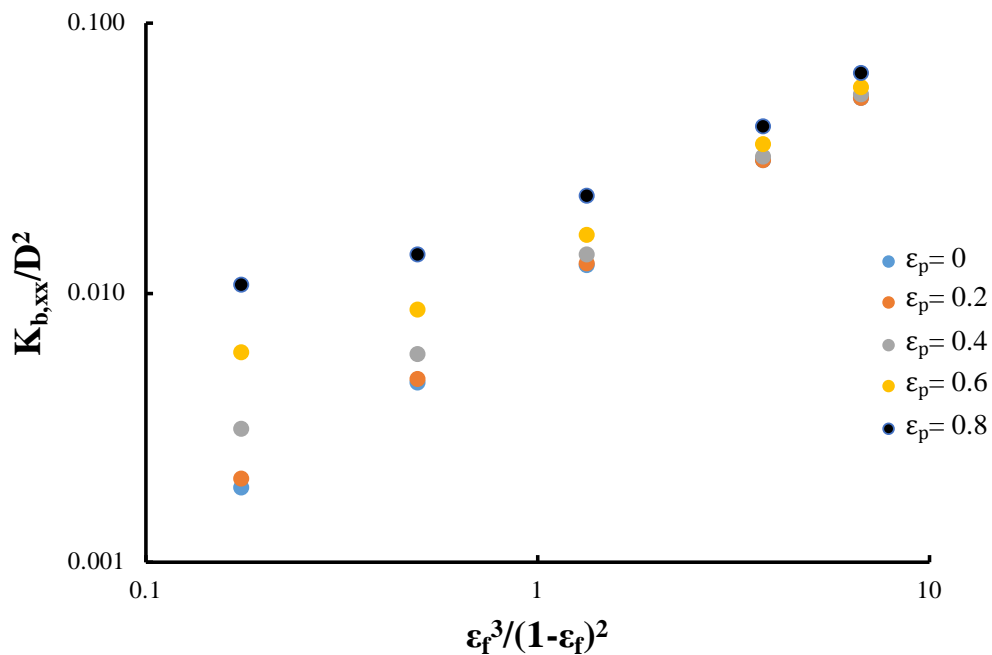


Figure 5.8. The change of $K_{b,xx} / D^2$ with $\varepsilon_f^3 / (1 - \varepsilon_f)^2$

5.2.2. Permeability in y Direction

Figure 5.9 shows the streamlines and pressure distributions in inter- and intraparticle pores of different dual scale porous media when fluid flows only in y direction. In the REV's shown in this figure, the intraparticle porosity is different while the interparticle porosity is constant as $\varepsilon_f = 0.75$. The main flow (interparticle flow)

occurs in the vertical direction and there are secondary flows in the right and left gaps between the particles. The main flow penetrates a little bit into the left and right gaps between the particles and distorts the secondary flows. As seen from the figures, the size of secondary flows in the left and right gaps between the particles is not affected by increasing the value of intraparticle porosity; however the size of vortices in the pores inside the particles changes with intraparticle porosity. One may find that the bulk permeability in y direction is almost identical for all dual scale porous media shown in Figure 5.9.

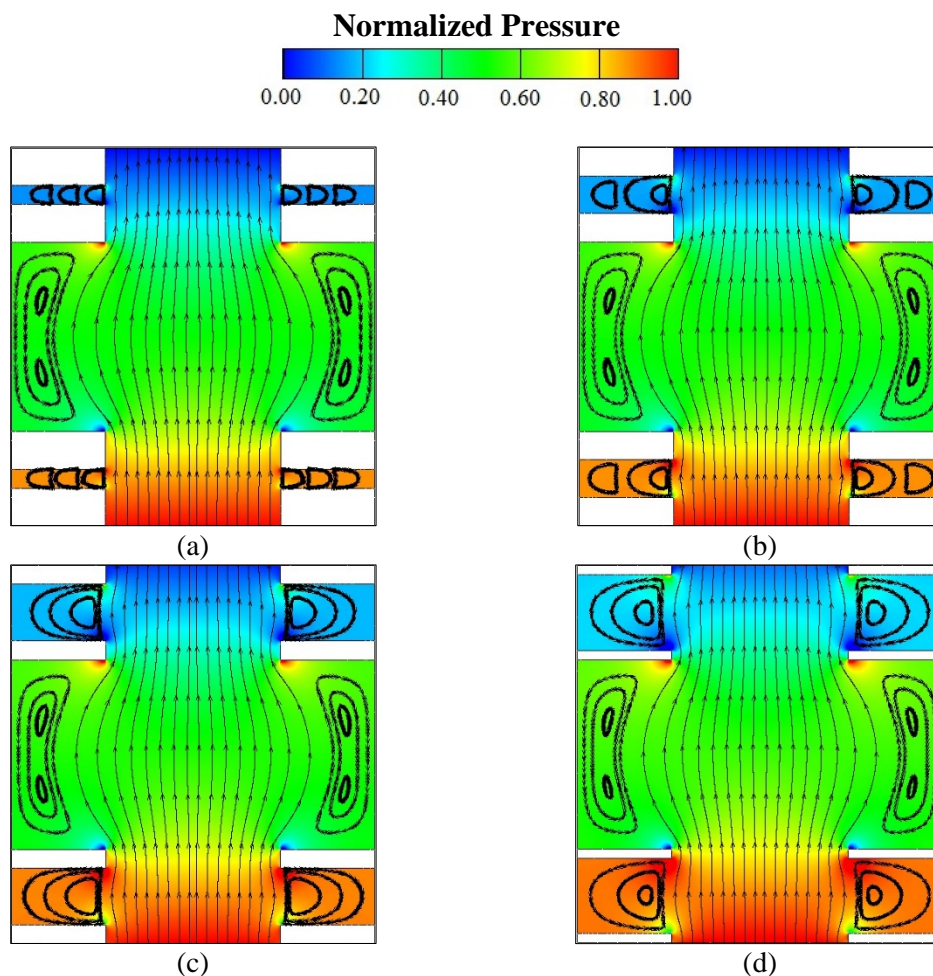


Figure 5.9. The streamlines and pressure contours for flow in y direction in dual scale porous media with $\varepsilon_f = 0.75$ a) $\varepsilon_p = 0.2$, b) $\varepsilon_p = 0.4$, c) $\varepsilon_p = 0.6$, d) $\varepsilon_p = 0.8$

Figure 5.10 shows the streamlines and pressure distribution in inter and intraparticle pores of different dual scale porous media in y direction. In these figures, intraparticle porosity changes while the interparticle porosity remains constant $\varepsilon_f = 0.4$. Although the increase of intraparticle permeability increases the area of the gap in

transverse direction of flow, it seems that the increase of ε_p does not have significant influence on the bulk permeability in y direction.

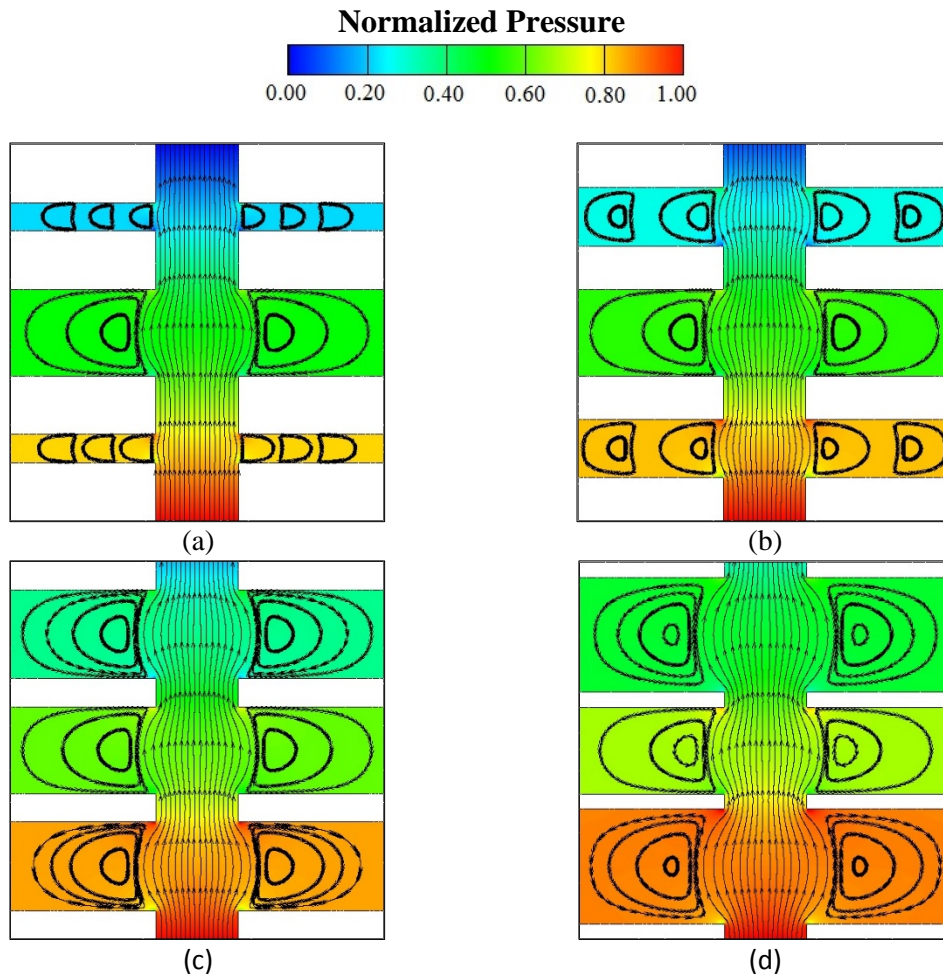


Figure 5.10. The streamlines and pressure contours for flow in y direction in dual scale porous media with $\varepsilon_f = 0.4$ a) $\varepsilon_p = 0.2$, b) $\varepsilon_p = 0.4$, c) $\varepsilon_p = 0.6$, d) $\varepsilon_p = 0.8$

Figure 5.11 indicates the variation between $K_{b,yy} / D^2$ and $\varepsilon_f^3 / (1 - \varepsilon_f)^2$ for different intraparticle porosities. As seen, the permeability in y direction is not influenced with the change of the intraparticle porosity and there is almost a linear variation between $K_{b,yy} / D^2$ and $\varepsilon_f^3 / (1 - \varepsilon_f)^2$ that enables the use of Kozeny-Carmen equation with constant Kozeny coefficient for determination of $K_{b,yy}$.

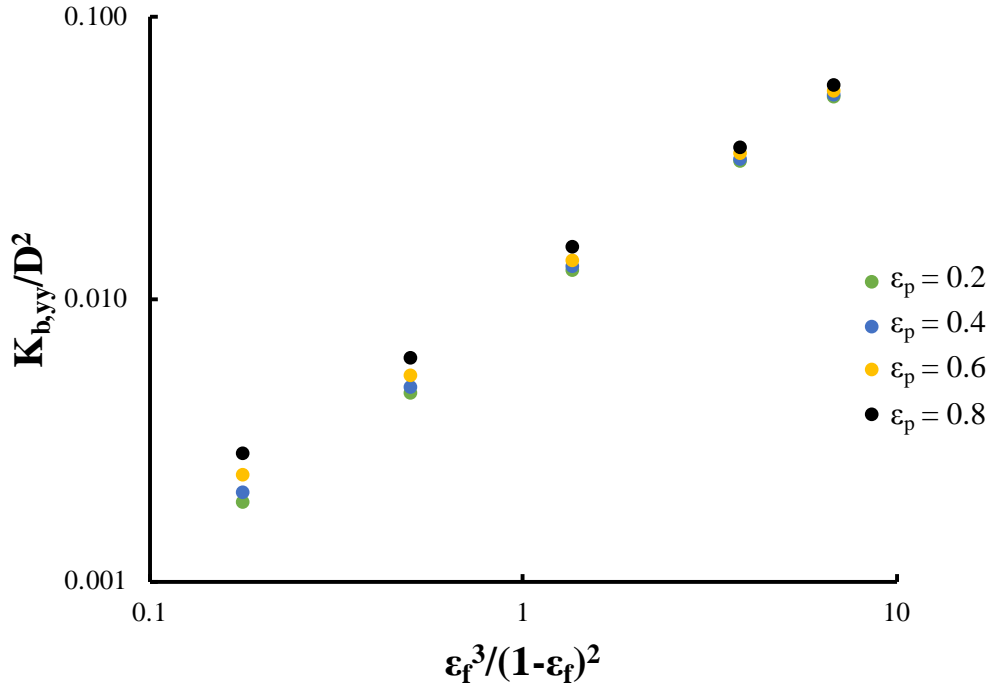


Figure 5.11. The change of $K_{b,yy} / D^2$ with $\epsilon_f^3 / (1 - \epsilon_f)^2$

5.3. Suggested Correlations

Based on the obtained results, Kozeny constant for x and y directions are calculated to find permeability value by using Kozeny-Carman equation. As it is well known, the Kozeny-Carman permeability relation was derived based on a porous medium consist of bundle of capillary channels with same radius. It can be defined as:

$$K = \frac{D^2 \epsilon_f^3}{16\kappa(1-\epsilon_f)^2} \quad (5.1)$$

where κ is called as Kozeny constant and it depends on porous media structure. In this study, based on obtained numerical results, Kozeny constant for x and y directions are found and presented in following part.

Kozeny constant for x direction:

A general equation for Kozeny constant based on the ratio of intra and interparticle permeability and intraparticle porosity is obtained. A proper mathematical relationship for the change of Kozeny constant in terms of the permeability ratio for $0.4 < \varepsilon_f < 0.75$ and $0.2 < \varepsilon_p < 0.8$ can be suggested as:

$$\kappa = A \left(\frac{K_{p,xx}}{K_{f,xx}} \right)^B \quad (5.2)$$

where A and B coefficients are constants and they are functions of intraparticle porosity and can be calculated from the following equation:

$$A = C_0 \varepsilon_p^3 + C_1 \varepsilon_p^2 + C_2 \varepsilon_p + C_3 \quad (5.3)$$

$$B = D_0 \varepsilon_p^3 + D_1 \varepsilon_p^2 + D_2 \varepsilon_p + D_3 \quad (5.4)$$

Based on the obtained pore level permeability values, the constant coefficients of equations (5.3) and (5.4) are obtained and given in Table 5.1.

Table 5.1. Empirical coefficients for determination of Kozeny constant
($0.4 < \varepsilon_f < 0.75$ and $0.2 < \varepsilon_p < 0.8$)

C ₀	4.246	D ₀	-0.112
C ₁	3.686	D ₁	-0.216
C ₂	3.115	D ₂	-0.393
C ₃	3.106	D ₃	-0.545

Figure 5.12 shows the comparison of the permeability values found by using the suggested Kozeny-Carman relation with the values obtained from the pore level simulation. A linear variation with the slope of 45° between $K_{b,xx}/D^2$ and $\varepsilon_f^3/\kappa(1-\varepsilon_f)^2$ should exist. As seen from the figure, the computed pore level permeability values with the suggested correlation have good agreement. The suggested relation for determination of Kozeny constant yields reasonable results for the calculation of permeability for ranges of interparticle porosity between 0.4 and 0.75 when the intraparticle porosity changes from 0.2 to 0.8.

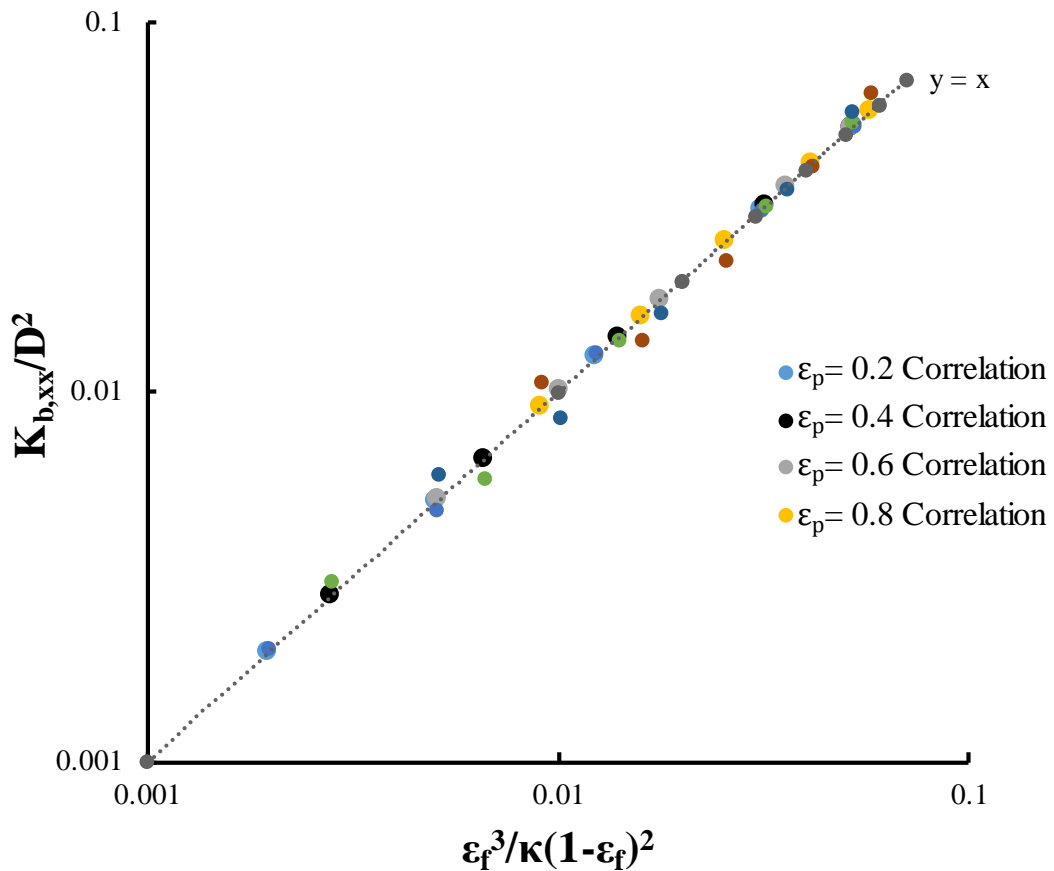


Figure 5.12. The comparison of suggested correlation in longitudinal direction with the obtained numerical permeability values

Kozeny constant for y direction:

As can be seen from Figure 5.11, the change of dimensionless bulk permeability with $\varepsilon_f^3/(1-\varepsilon_f)^2$ is almost linear and is not influenced from intraparticle porosity. That's why, the Kozeny constant is found as fixed value of 125. Figure 5.13 shows the comparison of the Kozeny relation (by using $\kappa = 125$) and obtained numerical values. As can be seen, the suggested Kozeny constant value is appropriate to provide value for permeability of the studied dual scale in y direction.

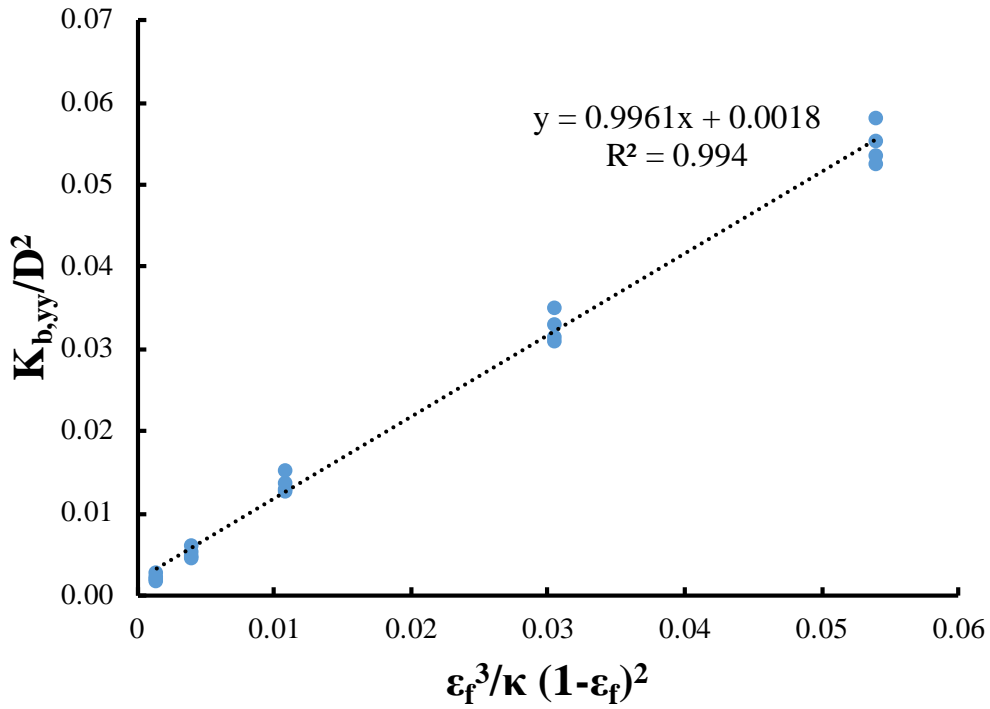


Figure 5.13. The comparison of the suggested equation for permeability in transverse direction with obtained numerical results

5.4. Results for Interfacial Convective Heat Transfer Coefficient

This part of study represents the effects of intraparticle porosity on the interfacial heat transfer coefficient for a periodic dual scale porous media containing inline array of square solid particles, numerically. Moreover the variation of Reynolds number and the intraparticle porosity are exhibited as well. In the literature review section the studies on the determination of the interfacial heat transfer coefficient by considering the impact of porosity, Re, particle arrangement and flow direction were presented. However, the effect of intraparticle porosity on the interfacial heat transfer coefficient was not studied for dual scale porous media. The results for microscopic velocity and temperature distributions in the voids between the rods are obtained by solving the continuity, Navier–Stokes, and energy equations for the representative elementary volume (REV). Based on the obtained microscopic temperature distributions, the interfacial convective heat transfer coefficients and the corresponding interfacial Nusselt numbers are computed. The study is performed for three interparticle porosity values of 0.75, 0.6 and 0.4 while the intraparticle porosity has changed from 0.2 to 0.75. It should be also mentioned that for each interparticle porosity, four cases with different size of intraparticle porosity is established. The

minimum value of ε_p is 0.2 for all interparticle porosity while the maximum value does not exceed the interparticle porosity values. In this study the Reynolds numbers are between 50 and 600.

5.4.1. Effects of Intraparticle Porosity on the Interfacial Nusselt Number

The streamlines and temperature contours for $\varepsilon_f = 0.75$ and 0.4 with different intraparticle porosities and different Reynolds numbers are displayed in Figure 5.14 and Figure 5.15. In order to compare different temperature fields, a dimensionless temperature definition is used as:

$$\langle \theta \rangle^f = \frac{\langle T \rangle^f - T_{\min}}{T_{\max} - T_{\min}} \quad (5.5)$$

where T_{\min} and T_{\max} are the minimum and maximum temperatures in the REV, respectively.

The streamlines and temperature distribution contours for $\varepsilon_f = 0.75$, $\varepsilon_p = 0.2$ and 0.75 are shown in Figure 5.14 for $Re = 50$ and 600 respectively. As can be seen from Figure 5.14 (a) and Figure 5.14 (c) three types of flow is observed in REV. The main flow passing through the interparticle region, the secondary flows occur in gaps between the solid particles and finally the fluid flow through intraparticle area. On the other hand the Figure 5.14 (b) and Figure 5.14 (d) illustrates that for $\varepsilon_p = 0.75$ the vortices has been disappeared due to the increasing size of intraparticle area. Hence, the stream through this region is more smooth and clear. The figures indicate that the temperature distribution considerably changes with Reynolds number. For the $Re = 50$ with $\varepsilon_p = 0.2$ the fluid temperature at the inlet of intraparticle region increase immediately to the solid temperature. However for $\varepsilon_p = 0.75$ the intraparticle region enhanced the heat transfer through the REV. Additionally, the fluid flow in the interparticle field of both 2 first cases create a thermal boundary layers on the horizontal surface of the solid particles which prevents the heat transfer in the transverse direction of the flow. Consequently the considerable temperature difference is achieved between the center and solid surface. From Figure 5.14 (c) and Figure 5.14 (d) as the Reynold

number increase ($Re = 600$) the velocity of the fluid is also increase which means that the residence time of the fluid particle in the REV decrease. As a result, the convection heat transfer becomes stronger and uniform temperature is observed. For the $Re = 600$ and $\varepsilon_p = 0.2$ the intraparticle porosity does not have the significant effect on the heat transfer but for $\varepsilon_p = 0.75$ the remarkable influence on the heat transfer can be seen as shown in Figure 5.14 (d).

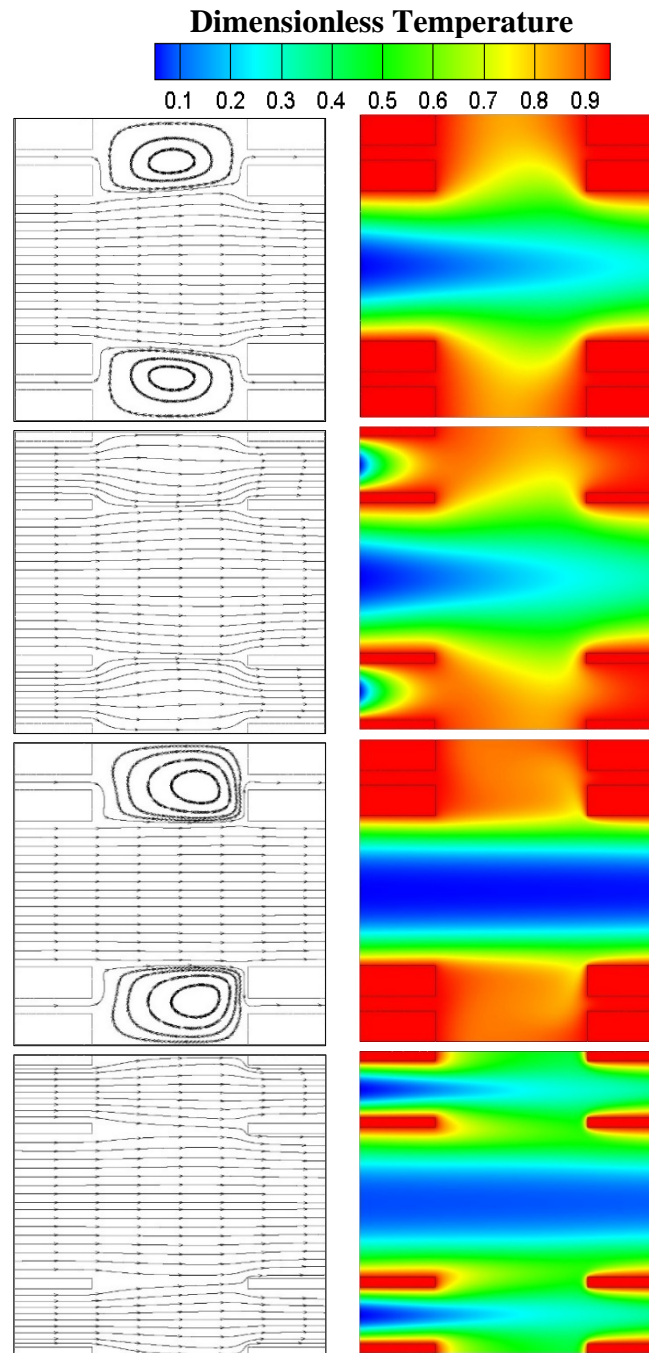


Figure 5.14. The streamlines (on the left) and temperature contours (on the right),
 (a) $\varepsilon_f = 0.75$, $\varepsilon_p = 0.2$, $Re = 50$, (b) $\varepsilon_f = 0.75$, $\varepsilon_p = 0.75$, $Re = 50$
 (c) $\varepsilon_f = 0.75$, $\varepsilon_p = 0.2$, $Re = 600$, (d) $\varepsilon_f = 0.75$, $\varepsilon_p = 0.75$, $Re = 600$

In Figure 5.15, for the values of $Re = 50$ and 600 the streamlines and temperature distribution contours for $\varepsilon_f = 0.4$ with ε_p changes between 0.2 and 0.4 are shown respectively. As can be seen from above figures, three types of flow is observed in REV with the same manner which were explained for Figure 5.14.

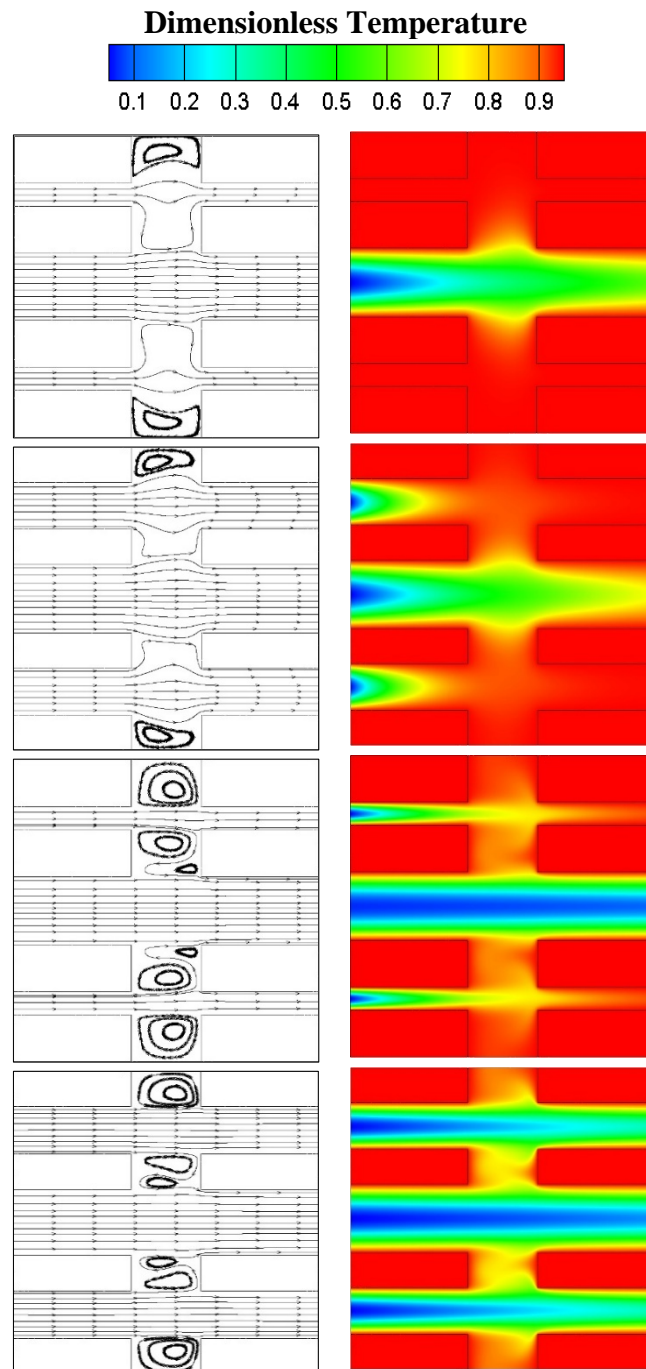


Figure 5.15. The streamlines (on the left) and temperature contours (on the right),
 (a) $\varepsilon_f = 0.4$, $\varepsilon_p = 0.2$, $Re = 50$, (b) $\varepsilon_f = 0.4$, $\varepsilon_p = 0.4$, $Re = 50$
 (c) $\varepsilon_f = 0.4$, $\varepsilon_p = 0.2$, $Re = 600$, (d) $\varepsilon_f = 0.4$, $\varepsilon_p = 0.4$, $Re = 600$

In Figure 5.15 (a) the effect of ε_p is not observed on the heat transfer. However for $\varepsilon_p = 0.4$ this effect is ascertained at the inlet of the structure. Additionally, Figure 5.15 (c) and (d) represent the velocity and temperature distribution for $Re = 600$. Besides the vortices at the very top and bottom of the REV, there are also vortices occur in the middle of structure between solid gaps. These vortices play an important role on the heat transfer and temperature distribution in the REV. Moreover, a strong strike of the fluid with the vertical edges of the outlet solid particles causes the penetration of the heat into the gaps. Therefore, the colder fluid enter into the gaps between the particles. Hence, the heat transfer on the vertical walls of the particles increases which is obvious for the intraparticle porosity of $\varepsilon_p = 0.4$ with $Re = 600$. Finally for $Re = 600$ due to the strong convective heat transport, the fluid temperature remains smaller than the solid temperature.

The variation of the interfacial Nu with intraparticle porosity for different Re values are shown in Figure 5.16. The interfacial Nu values change roughly between 5 and 23 for the studied interparticle porosity of 0.75.

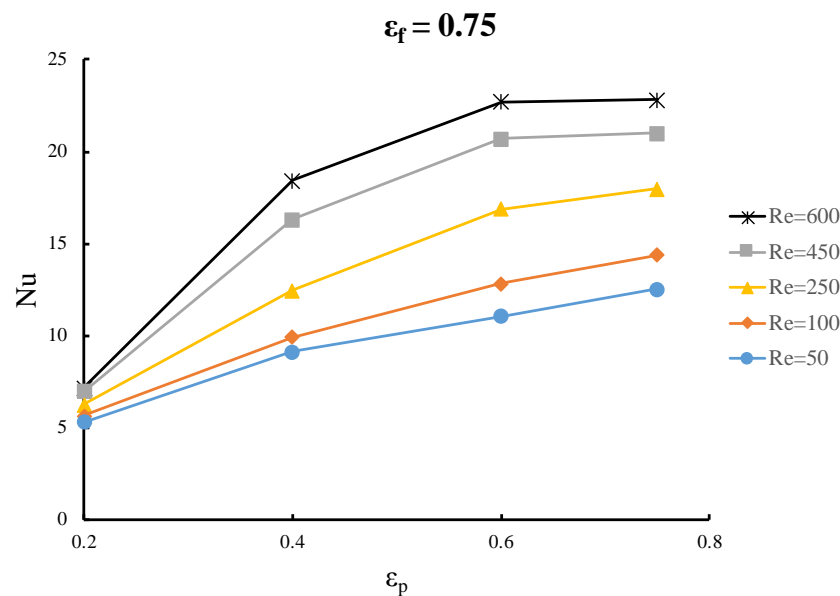


Figure 5.16. The variation of real Nu with ε_p for $\varepsilon_f = 0.75$ and different Re values

As can be seen from the figure the interfacial Nu number increases with ε_p due to the increase of the void space. The slight increase of Nu is observed for $Re = 50, 100, 250$ with $0.2 < \varepsilon_p < 0.75$. However for $Re = 450$ and 600 the changes is more dramatic

by changing the intraparticle porosity from 0.2 to 0.4. For intraparticle porosity of 0.6 and 0.75 the interfacial Nu is almost constant and similar to each other.

Figure 5.17 represents the interfacial Nu values for interparticle porosity 0.6 with ε_p changes between 0.2 and 0.6. For Re = 50, 100 and 250 the Nu values increase with respect to the change of intraparticle porosity. This increase is also observed for Re = 450 and 600 up to $\varepsilon_p = 0.4$ but for $\varepsilon_p = 0.6$ the slight decrease in Nu value ascertained.

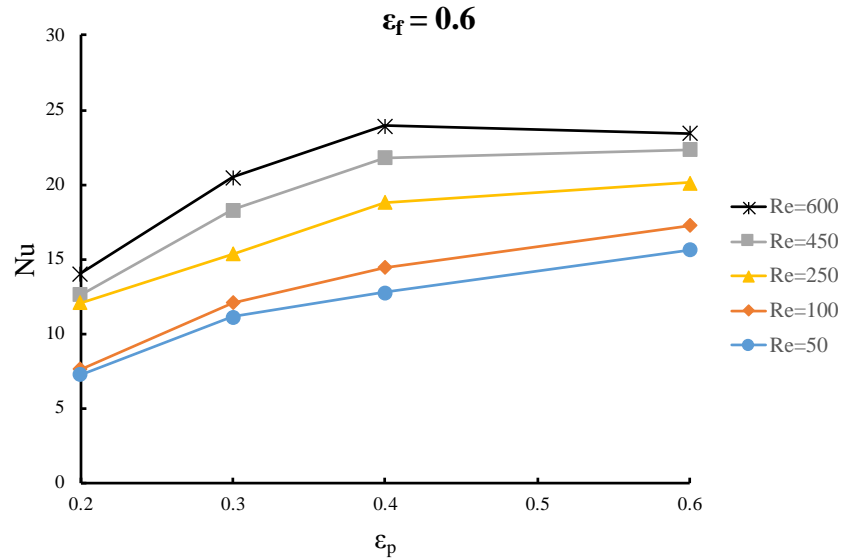


Figure 5.17. The variation of real Nu with ε_p for $\varepsilon_f = 0.6$ and different Re values

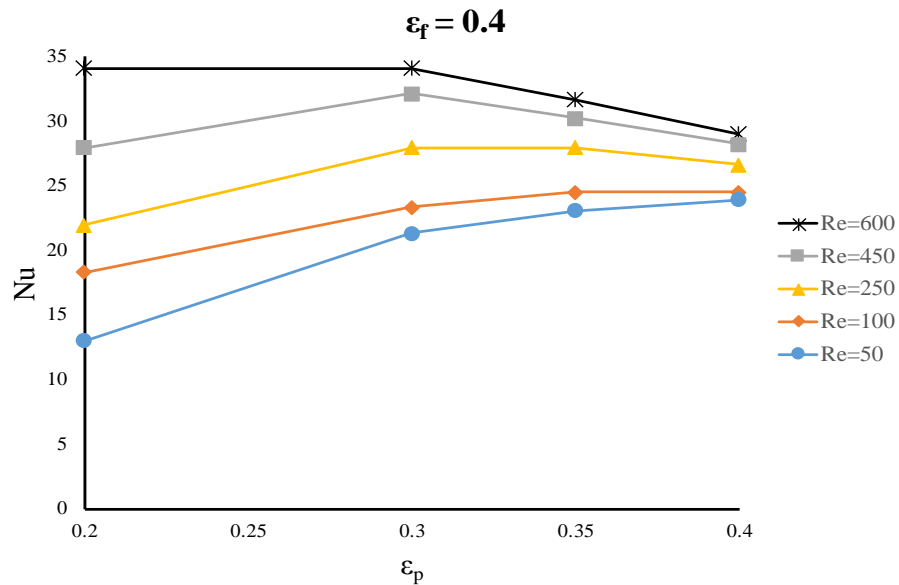
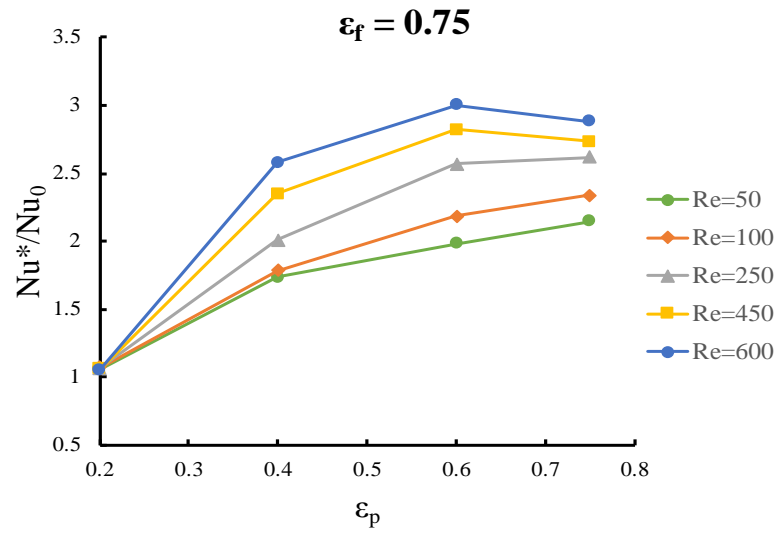


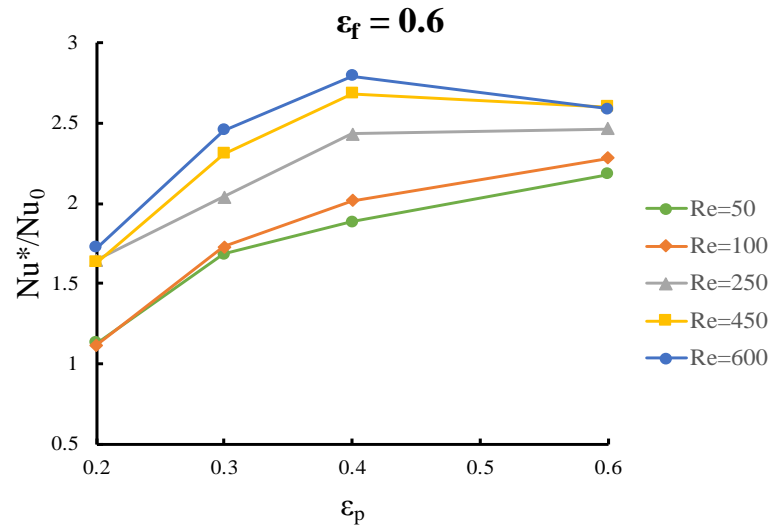
Figure 5.18. The variation of real Nu with ε_p for $\varepsilon_f = 0.4$ and different Re values

In Figure 5.18 the interparticle porosity is 0.4 while the rate of intraparticle porosity is from 0.2 to 0.4. The considerable increase is observed for all Re number by increase of ε_p from 0.2 to 0.3 except Re=600 which the value keeps constant. The small increment of Nu number is observed for Re = 50 and 100 with $\varepsilon_p > 0.3$. However, for Re = 250, 450, 600 and $\varepsilon_p = 0.35$ and 0.4 the considerable decrease of Nu number is seen.

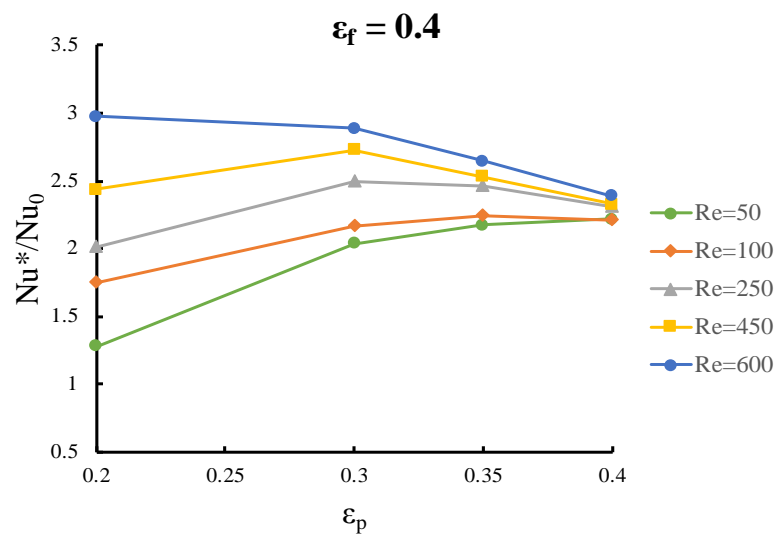
The ratio of modified Nusselt number* to Nu number of mono-scale porosity for three different interparticle porosity is shown in Figure 5.19. The figures clearly illustrate how the intraparticle porosity has an influences on Nu number. Moreover, it is observed that the change of Nu number is highly dependent on inter and intraparticle porosity and Re. As can be seen from Figure 5.19 (a) for $\varepsilon_f = 0.75$ the Nu number is increased by variation of intraparticle porosity. However for $\varepsilon_p = 0.2$ the increase rate is not considerable with respect to mono scale porous media. For Re = 50, 100 and 250 the increase rate of Nu is continues up to $\varepsilon_p = 0.75$ but for Re = 450 and 600 the maximum value of Nu is reached at $\varepsilon_p = 0.6$ and after that point a slight decrease of Nu is detected. Figure 5.19 (b) is related to interparticle porosity value of $\varepsilon_f = 0.6$. In this figure for $\varepsilon_p = 0.2$ and $\text{Re} \geq 250$ the great impact of intraparticle porosity on Nu number and interfacial convective heat transfer is determined. Additionally, the maximum values of Nu number for Re = 50 and 100 are observed at $\varepsilon_p = 0.6$, however for $\text{Re} \geq 250$ it occurs at $\varepsilon_p = 0.4$. Finally, Figure 5.19 (c) shows that for different value of Re number the increase rate of Nu number is noticeable. For instance, in dual scale porous media with $\varepsilon_f = 0.4$ ($\varepsilon_p = 0.4$) the Nu number value is 3 times greater than the mono scale porous medium which shows the important effect of intraparticle porosity on heat transfer.



(a)



(b)



(c)

Figure 5.19. The ratio of modified Nusselt number* to Nu number of mono scale porosity porous of media with a) $\varepsilon_f = 0.75$, b) $\varepsilon_f = 0.6$, c) $\varepsilon_f = 0.4$

CHAPTER 6

CONCLUSION

Fluid flow in a dual scale two dimensional porous media consisting of square rods are investigated, numerically. The continuity, Navier-stokes and energy equations both for intra and interparticle pores and entire REV of dual scale porous media are solved. The intrinsic permeability values and a correlation for determination of bulk permeability tensor is suggested. Based on the obtained results following remarks can be concluded:

- For flow in intraparticle pore direction (x direction), the increase of the intraparticle pore size removes gap between the particles and provides a fully straight flow. However, for flow in transverse direction (y direction), the increase of intraparticle pore size does not have important effect on flow patterns.
- The direction of intraparticle pores has important influence on the bulk permeability. Hence, correlations for determination of bulk permeability in terms of intraparticle porosity may not be accurate for heterogeneous porous media.
- The intraparticle porosity value increase the flow rate passes through the porous media and the particle becomes more permeable. However; for high interparticle porosity values such as 0.75, the intraparticle porosity does not have importance effect on bulk permeability.
- It seems that the equation of Kozeny–Carman is an appropriate relation for adaption onto dual scale porous media; however the Kozeny constant should be defined in terms of intra, interparticle permeability and porosity.
- The present study shows that the intraparticle porosity (ε_p) has an important effect on interfacial convective heat transfer coefficient. The increase of intraparticle porosity causes more fluid passes between and through the particles and consequently the interfacial Nusselt number increases. It seems that, the influence of low intraparticle porosity value (i.e., $\varepsilon_p = 0.2$) for high interparticle porosity values in a dual scale porous media is not noticeable on the interfacial Nusselt number and the heat transfer in the porous media behaves similar to the

fully developed heat transfer in a straight channel. For high values of ε_p the interfacial convective heat transfer coefficient increases for interparticle porosities of 0.75 and 0.6 however the opposite behavior is observed for the $\varepsilon_f = 0.4$ with $\varepsilon_p > 0.3$. The strike of the fluid to the vertical walls of the outlet solid particles and the entrance of fluid into the gaps between the particles may be the main reasons for this condition.

- Further increase of intraparticle porosity reduces the value of interfacial Nu number. Hence, for each ε_f as the Re number changes there is an optimum value of ε_p for maximization of heat transfer in dual scale porous media.
- The results of the present study can be used for many types of porous media such as fractured porous media, slotted fins and heat sinks since the effects of intraparticle porosity is important for these kind of porous media as well. The present study provides important hints for prediction of permeability, interfacial convective heat transfer and coefficient.

More investigations may be done on the different shapes and arrangements of dual scale porous media. Especially the analysis of heat and fluid flow in cylindrical types of dual scale porous medium with staggered arrangements would provide further understanding of the effect of intraparticle porosity on permeability and interfacial convective heat transfer coefficient.

REFERENCES

- ALSHARE, A. A., STRYKOWSKI, P. J. & SIMON, T. W. 2010. Modeling of unsteady and steady fluid flow, heat transfer and dispersion in porous media using unit cell scale. *International Journal of Heat and Mass Transfer*, 53, 2294-2310.
- BYON, C. & KIM, S. J. 2013. Permeability of Mono- and Bi-dispersed Porous Media. *EPJ Web of Conferences*, 45, 01018.
- CARMAN, P. C. 1937. Fluid flow through granular beds. *Chemical Engineering Research & Design: Transactions of the Institution of Chemical Engineers*, Part A, 415-421.
- DARCY, H. 1856. *Les fontaines publiques de la ville de Dijon*, Paris, Dalmont.
- DUPUIT, J. 1863. *Etudes theoretiques et pratiques sur le mouvement des eaux*, Paris, Dunond.
- FORCHHEIMER, P. H. 1901. Wasserbewegung durch Boden. *Z. Ver. Dtsch. Ing.*, 45, 1782-1788.
- GAMRAT, G., FAVRE-MARINET, M. & LE PERSON, S. 2008. Numerical study of heat transfer over banks of rods in small Reynolds number cross-flow. *International Journal of Heat and Mass Transfer*, 51, 853-864.
- HWANG, W. R. & ADVANI, S. G. 2010. Numerical Simulations of Stokes–Brinkman Equations for Permeability Prediction of Dual Scale Fibrous Porous Media. *Physics of Fluids*, 22, 113101.
- KAVIANY, M. 1995. *Principles of Heat Transfer in Porous Media*, New York, Springer-Verlag.
- KOZENY, J. 1927. Ueber kapillare Leitung des Wassers im Boden. *Sitzungsber Akad. Wiss.*, 136, 271-306.
- KUWAHARA, F., SHIROTA, M. & NAKAYAMA, A. 2000. A numerical study of interfacial convective heat transfer coefficient in two-energy equation model for convection in porous media. *International Journal of Heat and Mass Transfer*, 44, 1153-1159.
- LIU, S. & MASLIYAH, J. H. 2005. *Dispersion in Porous Media. Handbook of porous media*, Boca Raton, Taylor&Francis.
- LOPEZ PENHA, D. J., STOLZ, S., KUERTEN, J. G. M., NORDLUND, M., KUCZAJ, A. K. & GEURTS, B. J. 2012. Fully-developed conjugate heat transfer in porous media with uniform heating. *International Journal of Heat and Fluid Flow*, 38, 94-106.

- NABOVATI, A., LLEWELLIN, E. W. & SOUSA, A. C. M. 2010. Through-thickness permeability prediction of three-dimensional multifilament woven fabrics. *Composites Part A: Applied Science and Manufacturing*, 41, 453-463.
- NAKAYAMA, A. 1995. PC-Aided numerical heat transfer and convective flow. CRC Press.
- NAKAYAMA, A., KUWAHARA, F. & SANO, Y. 2007. Concept of equivalent diameter for heat and fluid flow in porous media. *AIChE Journal*, 53, 732-736.
- NAKAYAMA, A., KUWAHARA, F., UMEMOTO, T. & HAYASHI, T. 2002. Heat and Fluid Flow Within an Anisotropic Porous Medium. *Journal of Heat Transfer*, 124, 746.
- NEDANOV, P. B. & ADVANI, S. G. 2002. Numerical Computation of the Fiber Preform Permeability Tensor by the Homogenization Method. *Polymer Composites*, 23, 758-770.
- NGO, N. D. & TAMMA, K. K. 2001. Microscale Permeability Predictions of Porous Fibrous Media. *International Journal of Heat and Mass Transfer*, 44, 3135-3145.
- NIELD, D. A. & BEJAN, A. 2006. *Convection in porous media*, U.S., Springer.
- NIELD, D. A. & KUZNETSOV, A. V. 2011. Forced Convection in a Channel Partly Occupied by a Bidisperse Porous Medium: Symmetric Case. *Journal of Heat Transfer*, 133, 072601.
- OZGUMUS, T. & MOBEDI, M. 2014. Effect of Pore to Throat Size Ratio on Interfacial Heat Transfer Coefficient of Porous Media. *Journal of Heat Transfer*, 137, 012602.
- OZGUMUS, T., MOBEDI, M. & OZKOL, U. 2014. Determination of Kozeny Constant Based On Porosity and Pore to Throat Size Ratio in Porous Medium with Rectangular Rods. *Engineering Applications of Computational Fluid Mechanics*, 8, 308-318.
- PAPATHANASIOU, T. D. 2001. Flow Across Structured Fiber Bundles: A Dimensionless Correlation. *International Journal of Multiphase Flow*, 27, 1451-1461.
- RANGANATHAN, S. 1996. A Generalized Model for the Transverse Fluid Permeability in Unidirectional Fibrous Media. *Polymer Composites*, 17, 222-230.
- SAADA, M. A., CHIKH, S. & CAMPO, A. 2005. Analysis of hydrodynamic and thermal dispersion in porous media by means of a local approach. *Heat and Mass Transfer*, 42, 995-1006.

- SAITO, M. B. & DE LEMOS, M. J. S. 2006. A Correlation for Interfacial Heat Transfer Coefficient for Turbulent Flow Over an Array of Square Rods. *Journal of Heat Transfer*, 128, 444.
- SINGH, M. & MOHANTY, K. K. 2000. Permeability of spatially correlated porous media. *Chemical Engineering Science*, 55, 5393-5403.
- TAHIR, M. W., HALLSTRÖM, S. & ÅKERMO, M. 2014. Effect of Dual Scale Porosity on the Overall Permeability of Fibrous Structures. *Composites Science and Technology*, 103, 56-62.
- TERUEL, F. E. & RIZWAN, U. 2009. Characterization of a porous medium employing numerical tools: Permeability and pressure-drop from Darcy to turbulence. *International Journal of Heat and Mass Transfer*, 52, 5878-5888.
- TUNG, K. L., SHIAU, J. S., CHUANG, C. J., LI, Y. L. & LU, W. M. 2002. CFD analysis on fluid flow through multifilament woven filter cloths. *Separation Science and Technology*, 37, 799-821.
- VAFAI, K. & TIEN, C. L. 1981. Boundary and inertia effects on flow and heat transfer in porous media. *International Journal of Heat and Mass Transfer*, 24, 195-203.
- WANG, Q., MAZÉ, B., VAHEDITAFRESHI, H. & POURDEYHIMI, B. 2006. A note on permeability simulation of multifilament woven fabrics. *Chemical Engineering Science*, 61, 8085-8088.
- WHITAKER, S. 1999. *The Method of Volume Averaging*, Dordrecht, The Netherlands, Kluwer Academic.
- XU, P. & YU, B. 2008. Developing a new form of permeability and Kozeny–Carman constant for homogeneous porous media by means of fractal geometry. *Advances in Water Resources*, 31, 74-81.
- YANG, J., WANG, Q., ZENG, M. & NAKAYAMA, A. 2010. Computational study of forced convective heat transfer in structured packed beds with spherical or ellipsoidal particles. *Chemical Engineering Science*, 65, 726-738.
- YU, B. & CHENG, P. 2002. A Fractal Permeability Model for Bi-dispersed Porous Media. *International Journal of Heat and Mass Transfer*, 45, 2983-2993.